GEOPHYSICS, VOL. 35, NO. 5 (OCTOBER 1970), P. 862–896, 31 FIGS.

ELECTROMAGNETIC FIELDS ABOUT A LOOP SOURCE OF CURRENT†

JISOO RYU, H. FRANK MORRISON,* AND STANLEY H. WARD‡

Integral expressions for the electromagnetic field components produced by a horizontal loop, carrying a current $Ie^{i\omega t}$ and placed on or above the surface of an n-layered half-space, are deduced in a form such that numerical integration can be performed easily. The expressions are free of approximations and completely general for all frequencies. They are constrained only to the uniformity of current around the transmitting loop. The resulting computed electromagnetic fields are valid for arbitrary values of the electrical parameters σ, μ, and ϵ. The quasi-static approximation for the region above the half-space, wherein the wave equation is replaced by the Laplace equation, can be avoided.

Measurements outside the loop constitute *induction depth sounding*. Induction depth sounding curves of field components and magnetic polarization parameters show good resolution of subsurface layering. In particular, it is suggested that the measurements of tilt angle and/or ellipticity of the magnetic polarization ellipse should be made to determine earth layering because of the rapidity and ease of these measurements in field operation. It is shown that the radius of the loop should, in the general case, be taken into account in theoretical computations.

Measurements at the center of the loop constitute *central induction sounding*. Central induction sounding responses are diagnostic only for layered earth models in which conductivity increases with depth. Measurement of the quadrature part of the vertical magnetic field is particularly promising.

Theoretical curves for earth models consisting of one layer overlying a half-space are given for the quasi-static case for induction depth sounding, and for the *nonquasi-static* (general) case for central induction sounding.

In another application, the response from a homogeneous, conductive, magnetic half-space with the central induction method at low frequencies reveals the feasiblity of in-situ determination of static magnetic permeability.

In a final application, it is shown that the effect of ground conductivity should be included in making the *normal* correction to Turam data whenever the apparent conductivity of the ground is greater than 10^{-3} mhos/m.

INTRODUCTION

The primary objective of this paper is the development of complete solutions for the electromagnetic field components due to a horizontal current-carrying loop of finite radius situated on or above the surface of an n-layered earth in such a way that numerical computations can be readily achieved for any source-detector configuration and for any source frequency. The mathematical formulation in general follows the integral expressions given by Morrison, Phillips, and O'Brien (1969), but overcomes the impracticality of numerical evaluation of their solutions when the loop is on or close to the surface of the earth. The solutions outside and at the center of the loop are applied to electromagnetic depth sounding and central induction sounding, respectively, of layered earth structures in exploration for ground water and possibly for petroleum.

No general solution for the fields over a stratified earth of a loop of finite radius appears in the literature although discussions pertaining to a

† Manuscript received by the Editor January 26, 1970; revised manuscript received May 21, 1970.

* Engineering Geoscience, University of California, Berkeley, California 94720.

‡ Department of Geological and Geophysical Sciences, University of Utah, Salt Lake City, Utah 84112.

loop of infinitesimal radius are frequent. To mention two, Vanyan (1967) gave rigorous mathematical details leading to the analytical expressions for field components from a dipolar source, while Frischknecht (1967) tabulated mutual coupling ratios, which assist in the quantitative interpretation of electromagnetic data for various source-detector configurations over two-layered earth models. We note that theoretical aspects and interpretation schemes for the central induction method were discussed by Yoshizumi et al (1959), Kosenkov (1963), and Patra (1969). In all of the above work, several approximations, including the quasi-static assumption (Wait, 1951), have been employed. The neglect of displacement current in the ground and/or in the air may not be valid for certain geologic environments and/or frequencies higher than 5×10^4 hz (Hohmann and Ward, 1968). However, it is recognized that the quasi-static solutions do permit the introduction of displacement currents in the ground (Wait, 1958 and Ward, 1969). In fact, Wait (1952) and Bhattacharyya (1959 and 1963) developed solutions for the electromagnetic fields of a dipolar source, taking into account the effect of both conduction and displacement currents in the ground. The expressions for a loop source of current developed in our paper are complete and perfectly general for all frequencies in any horizontally layered geologic environment. The only limitation in this analysis is that the dimension of the transmitting loop should be sufficiently small in comparison with the wavelength in free space to have the current uniform around the loop.

Two other applications of loop solutions will be presented. First, the theoretical response of a homogeneous, conductive, magnetic half-space indicates a possible way that the static magnetic permeability can be determined in situ and in the laboratory. Mooney (1952) developed an induction bridge instrument for the measurement of magnetic susceptibility in situ. Subsequently, Mooney and Bleifuss (1953) and Hood and Sangster (1967) used an in-situ susceptibility meter of this type in regional susceptibility mapping. Our solutions show that susceptibility may easily be obtained from field measurements via the central induction method. Second, the *normal* correction for the Turam method is shown to be dependent upon the apparent conductivity of the ground. The detailed aspects of Turam are presented in an article by Bosschart (1964) to which the reader is referred for a basis for appraisal of the significance of the comments we make with respect to the method.

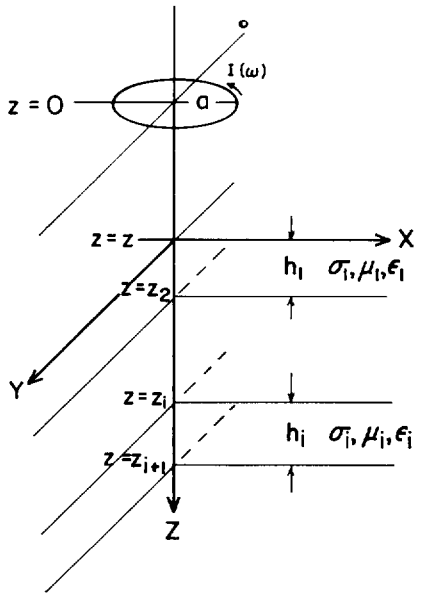

FIG. 1. Geometry of coordinate system.

THEORETICAL BASIS FOR COMPUTATION

Fields exterior to the loop

The integral expressions for the electromagnetic field generated by a finite loop will be developed for the case of a transmitting loop elevated at a height of z meters above an n-layered half-space. The expressions are, of course, valid when the loop is on the ground. We will assume mks units and $e^{i\omega t}$ excitation throughout. The geometry of the coordinate system is shown in Figure 1.

The circular symmetry allows us to employ a cylindrical coordinate system, reducing Maxwell's equations to the following:

$$i\omega\mu_i H_r = \frac{\partial E_\theta}{\partial z}, \tag{1}$$

$$i\omega\mu_i H_z = -\frac{1}{r}\frac{\partial}{\partial r}(rE_\theta), \tag{2}$$

and

$$\frac{\partial H_r}{\partial z} - \frac{\partial H_z}{\partial r} = (i\omega\epsilon_i + \sigma_i)E_\theta + J_{s\theta}, \tag{3}$$

where the source current density is given by the expression

$$J_{s\theta} = \frac{I(\omega)a\delta(r-a)\delta(z)}{r}\theta \cdot \tag{4}$$

In equation (4) we have treated the current loop as a summation of infinitesimal electric dipoles around the loop. The parameters σ_i, ϵ_i, and μ_i are the conductivity, dielectric permittivity, and magnetic permeability, respectively, of the ith layer. The notation $\delta(\cdot)$ signifies the Dirac delta function.

By eliminating H_r and H_z from equations (1), (2), and (3), we obtain an inhomogeneous scalar equation,

$$\left(\frac{\partial^2}{\partial z^2}+\frac{\partial^2}{\partial r^2}+\frac{1}{r}\frac{\partial}{\partial r}-\frac{1}{r^2}+k^2\right) \cdot E_\theta(r, z, \omega) = \frac{i\omega\mu_0 I(\omega)\delta(r-a)\delta(z)}{r}, \tag{5}$$

where $k_i^2=\omega^2\mu_i\epsilon_i-i\omega\mu_i\sigma_i$. The subscript o refers to parameters in free space. The source term in equation (5) disappears in all layers except for the free space containing the loop. By Hankel and Fourier transformations and subsequent inversion of the Fourier transformation by contour integration, equation (5) yields for the primary field in Hankel-transformed λ-space,

$$E_\theta(\lambda, z, \omega) = -\frac{i\omega\mu_0 aI(\omega)}{2} J_1(\lambda a)\frac{e^{-u_0 z}}{u_0}, \tag{6}$$

where $u_i=(\lambda^2-k_i^2)^{1/2}$ and $J_1(\cdot)$ is the first order Bessel function.

From equation (6), Morrison et al (1969) obtained the secondary electric field at the horizontal distance r from the center of the loop by matching solutions at the boundaries and introducing the input impedance concept. Morrison et al wrote

$$E_s(r, z, \omega) = -i\omega\mu_0 aI(\omega) \cdot \int_0^\infty \frac{e^{-u_0 z}}{u_0}\frac{Z^1}{Z_0+Z^1}J_1(\lambda a)J_1(\lambda r)\lambda d\lambda, \tag{7}$$

where the input impedance of the ith layer is given by (Wait, 1962)

$$Z^i = Z_i\frac{Z^{i+1}+Z_i\tanh(u_i h_i)}{Z_i+Z^{i+1}\tanh(u_i h_i)}, \tag{8}$$

and the intrinsic impedance Z_i is defined as

$$Z_i = -\frac{i\omega\mu_i}{u_i}. \tag{9}$$

For a semi-infinite bottom layer, we note that $Z^n=Z_n$.

Let us examine the improper integral of equation (7). When z becomes zero, which is the case for the loop placed on the earth's surface, a severe oscillation of the integrand is observed due to the two Bessel functions. This makes the simple numerical integration of equation (7) impractical. However, it can be observed that

$$\lim_{\lambda\to\infty}\frac{e^{-u_0 z}}{u_0}\frac{Z^1}{Z_0+Z^1}J_1(\lambda a)J_1(\lambda r)\lambda \to \frac{e^{-\lambda z}}{2}J_1(\lambda a)J_1(\lambda r)$$

as λ becomes sufficiently large. In order to make the integrand definitely converge, even though very slowly, without regard to the nature of the first order Bessel function, equation (7) can be written as

$$\begin{aligned} E_s(r, z, \omega) &= -i\omega\mu_0 aI(\omega)\left\{\int_0^\infty\left(\frac{e^{-u_0 z}}{u_0}\frac{Z^1}{Z_0+Z^1}\lambda - \frac{e^{-\lambda z}}{2}\right)J_1(\lambda a)J_1(\lambda r)d\lambda\right. \\ &\left. + \int_0^\infty \frac{e^{-\lambda z}}{2}J_1(\lambda a)J_1(\lambda r)d\lambda\right\}. \end{aligned} \tag{10}$$

Then, the first integral expression can be evaluated numerically. The second improper integral can be reduced to a finite integral by use of a relation given by Watson (1966) as follows:

$$\begin{aligned} &\int_0^\infty e^{-at}t^{\mu-\nu}J_\mu(bt)J_\nu(ct)dt \\ &= \frac{(\frac{1}{2}b)^\mu(\frac{1}{2}c)^\nu\Gamma(2\mu+1)}{\Gamma(\nu+\frac{1}{2})\Gamma(\frac{1}{2})}\int_0^\pi \cdot \frac{\sin^{2\nu}\phi d\phi}{(a^2+2iac\cos\phi-c^2\cos^2\phi+b^2)^{\mu+1/2}}. \end{aligned} \tag{11}$$

Equation (11) is applicable for real $(a+ib+ic)>0$

and real $(\mu) > -\frac{1}{2}$, where $\Gamma(\cdot)$ is a gamma function. Equation (10) reduces to

$$E_s(r, z, \omega) = -i\omega\mu_0 a I(\omega) \left\{ \int_0^\infty \left(\frac{e^{-u_0 z}}{u_0} \frac{Z^1}{Z_0 + Z^1} \lambda - \frac{e^{-\lambda z}}{2} \right) J_1(\lambda a) J_1(\lambda r) d\lambda + \frac{ar}{2\pi} \int_{-1}^{1} \text{Real} \left[\frac{(1 - x^2)^{1/2}}{(z^2 + 2iazx - a^2x^2 + r^2)^{3/2}} \right] dx \right\}. \tag{12}$$

There are two points to be mentioned about the second integral: (a) it is valid only when $z>0$ due to the conditions imposed on equation (11), although we found that z could be safely set to zero for the present problem by considering it as a limiting case, and (b) there is no singularity as long as $r>a$.

The H_r and H_z components can be deduced from equations (1), (2), and (12), as follows:

$$H_r(r, z, \omega) = aI(\omega) \left\{ \int_0^\infty \left(e^{-u_0 z} \frac{Z^1}{Z_0 + Z^1} - \frac{e^{-\lambda z}}{2} \right) J_1(\lambda a) J_1(\lambda r) \lambda d\lambda + \frac{3ar}{2\pi} \int_{-1}^{1} \text{Real} \left[\frac{(1 - x^2)^{1/2}(z + iax)}{(z^2 + 2iazx - a^2x^2 + r^2)^{5/2}} \right] dx \right\}, \tag{13}$$

and

$$H_z(r, z, \omega) = aI(\omega) \left\{ \int_0^\infty \left(\frac{e^{-u_0 z}}{u_0} \frac{Z^1}{Z_0 + Z^1} \lambda - \frac{e^{-\lambda z}}{2} \right) J_1(\lambda a) J_0(\lambda r) \lambda d\lambda + \frac{a}{\pi} \int_{-1}^{1} \text{Real} \left[\frac{(1 - x^2)^{1/2}}{(z^2 + 2iazx - a^2x^2 + r^2)^{3/2}} \right] dx - \frac{3ar^2}{2\pi} \int_{-1}^{1} \text{Real} \left[\frac{(1 - x^2)^{1/2}}{(z^2 + 2iazx - a^2x^2 + r^2)^{5/2}} \right] dx \right\}. \tag{14}$$

Thus, equations (12), (13), and (14) yield all components of the electromagnetic field outside the current-carrying finite loop. They depend upon the electrical parameters of the ground as well as the geometric parameters, a, r, and z. Setting $z=0$ in the equations reduces the solutions to the case of the loop on the surface of an n-layered half-space.

Fields at the center of the loop

At the center of the loop, only the vertical component of magnetic field will be observed in the absence of any lateral inhomogeneity; the radial component of magnetic field and the tangential component of electric field vanish.

The vertical component of magnetic field at the center of the loop is written in the Hankel-transformed λ-space as

$$H_z(0, z, \omega) = aI(\omega) \cdot \int_0^\infty \frac{e^{-u_0 z}}{u_0} \frac{Z^1}{Z_0 + Z^1} J_1(\lambda a) \lambda^2 d\lambda. \tag{15}$$

Again, equation (15) can be altered, for an assurance of the convergence of the integrand, to

$$H_z(0, z, \omega) = aI(\omega) \cdot \left\{ \int_0^\infty \left(\frac{e^{-u_0 z}}{u_0} \frac{Z^1}{Z_0 + Z^1} \lambda - \frac{e^{-\lambda z}}{2} \right) J_1(\lambda a) \lambda d\lambda + \int_0^\infty \frac{e^{-\lambda z}}{2} J_1(\lambda a) \lambda d\lambda \right\}. \tag{16}$$

The first improper integral can be evaluated numerically and the second part can be evaluated

analytically, taking advantage of the following relations:

$$-\frac{\partial}{\partial a}J_0(\lambda a) = J_1(\lambda a)\lambda \tag{17}$$

and

$$\int_0^\infty e^{-\lambda z}J_0(\lambda a)d\lambda = \frac{1}{(a^2+z^2)^{1/2}}, \quad z > 0. \tag{18}$$

Equation (16) becomes

$$H_z(o, z, \omega) = aI(\omega) \cdot \int_0^\infty \left(\frac{e^{-u_0 z}}{u_0}\frac{Z^1}{Z_0 + Z^1}\lambda - \frac{e^{-\lambda z}}{2}\right)J_1(\lambda a)\lambda d\lambda + \frac{a^2 I(\omega)}{2(a^2 + z^2)^{3/2}}. \tag{19}$$

We note from equation (19) that, as frequency becomes zero, the first term vanishes and the remaining second term represents the static field in the air.

In the actual numerical integration of the improper integrals of equations (12), (13), (14), and (19), the nonlinear transformation discussed by Gray and Atchison (1967) and Atchison and Gray (1968) was utilized to accelerate the convergence of the integrands. The essence of the nonlinear transformation is given in Appendix A.

APPLICATIONS

General

The mathematical formulation developed in the preceding section can find its applications in induction depth sounding, in central induction sounding, in measurement of magnetic susceptibility in situ, and in obtaining the *normal* correction for Turam. Measurements outside a transmitting loop are pertinent to induction depth sounding, while those at the center of the loop are pertinent to central induction sounding. In the following computations, the magnitude of the magnetic dipole moment[1] of the transmitting loop is assumed to be unity. Unless otherwise indicated, free space values of dielectric constant and magnetic permeability are assumed.

While in field practice a square or rectangular loop probably would be used for the applications noted above, the theoretical solutions for a circular loop are easier to compute and are adequate for most purposes.

[1] The dipole moment is defined by $m = \pi a^2 NI$ in which N is the number of turns of wire of a loop, a is the radius of the loop, and the current flowing in the loop is $Ie^{i\omega t}$

Induction depth sounding

Recently, electromagnetic depth sounding has attracted attention for both petroleum and ground water exploration. The sounding can be accomplished by varying either the source frequency (parametric sounding) or the source-detector distance (geometric sounding). The parametric technique has an advantage over the geometric technique in that the geologic noise from lateral inhomogeneities is considerably reduced. Also, especially for deep penetration, the field work is simpler and less expensive for parametric sounding. These advantages are worth the instrumental complications of parametric sounding. Thus, emphasis will be placed on this sounding technique.

Parameters measured. Measurements of 10 field quantities have been envisioned here. They are the modulus and the phase of the horizontal electric field (E_s), the modulus and phase of the horizontal magnetic field (H_r), the modulus and phase of the vertical magnetic field (H_z), plus 4 polarization parameters of the magnetic polarization ellipse, namely, the modulus and the phase of wave tilt, the tilt angle, and the ellipticity. The general layout of the sounding system and the orientation of the magnetic polarization ellipse are depicted in Figure 2a. The sign convention of the tilt angle is described in Figure 2b. With reference to Figure 2a, the above quantities can be written as:

$$E_s = |E_s| e^{i\phi_s},$$
$$H_r = |H_r| e^{i\phi_r},$$
$$H_z = |H_z| e^{i\phi_z},$$
$$\text{Wave tilt} = \frac{H_r}{H_z} = \left|\frac{H_r}{H_z}\right| e^{i\phi_t}, \quad \phi_t = \phi_r - \phi_z,$$
$$\text{Tilt angle} = \alpha = \tan^{-1}\left(\frac{-B + (B^2 + 4A^2)^{1/2}}{2A}\right),$$
$$A = |H_r||H_z| \cos(\phi_r - \phi_z),$$
$$B = |H_r|^2 - |H_z|^2,$$
$$0 \le \alpha < \pi,$$

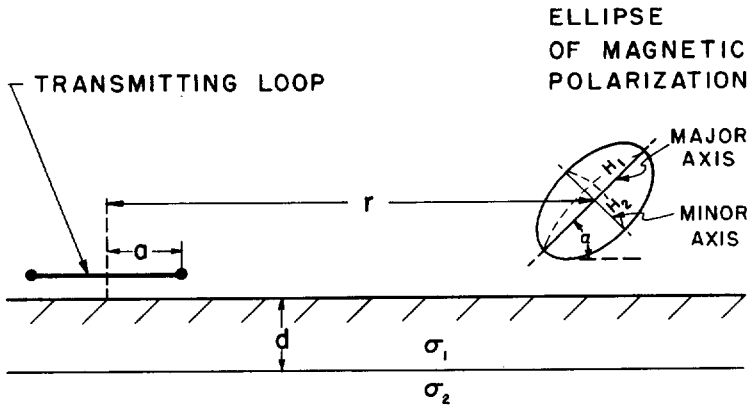

FIG. 2a. Section view of magnetic polarization ellipse.

$$\text{Ellipticity} = \frac{|H_2|}{|H_1|}.$$

The shape of the magnetic polarization ellipse can be completely characterized by two polarization parameters, that is, tilt angle and ellipticity. In actual field measurements, the magnetic polarization parameters are often much easier and faster to measure than the field components, which require stable, precise instrumentation.

Equations (12), (13), and (14) yield the complete (*nonquasi-static*) expressions for the field components. However, the quasi-static approximation, in which the displacement currents in both the air and the ground are neglected, can be applied to most earth models (Wait, 1951). We may represent the wavenumber as

$$k = (\omega^2\mu\epsilon - i\omega\mu\sigma)^{1/2} = \left[-i\omega\mu\sigma\left(1 + \frac{i}{\tan\delta}\right)\right]^{1/2},$$

where $\tan\delta$ is the loss tangent. The quasi-static approximation is valid for the cases where $\tan\delta$ is far greater than unity and the operating frequency is less than 5×10^4 hz (Hohmann and Ward, 1968). Neglect of displacement currents in the air is an acceptable approximation provided the source-detector separation is much less than a free space wavelength at the operating frequency (Wait, 1954). These two approximations are generally true for most active electromagnetic systems used in exploration. Upon introducing the quasi-static assumption, we find that the electromagnetic responses will depend upon a dimensionless induction number defined by $B = (\omega\mu\sigma_1/2)^{1/2}r$, where σ_1 is the conductivity of the top layer. The range of the induction numbers over which the electromagnetic responses appear most interesting and diagnostic of subsurface electrical layering is from about 0.1 to 10. In the computations for parametric sounding, the operating frequencies are so chosen that the induction number falls in the range between 0.1 to 10. Hence, the field quantities are plotted over that range of the induction number.

Parametric sounding, conductivity increasing with depth. A two-layered earth model, designated

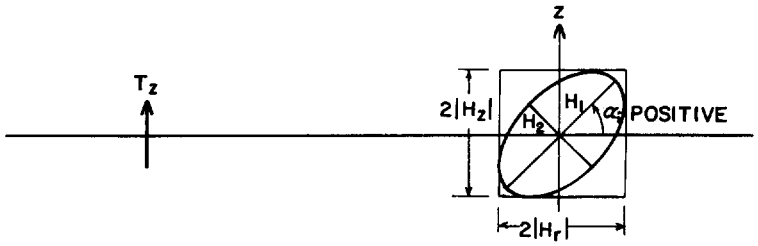

FIG. 2b. Sign convention of tilt angle.

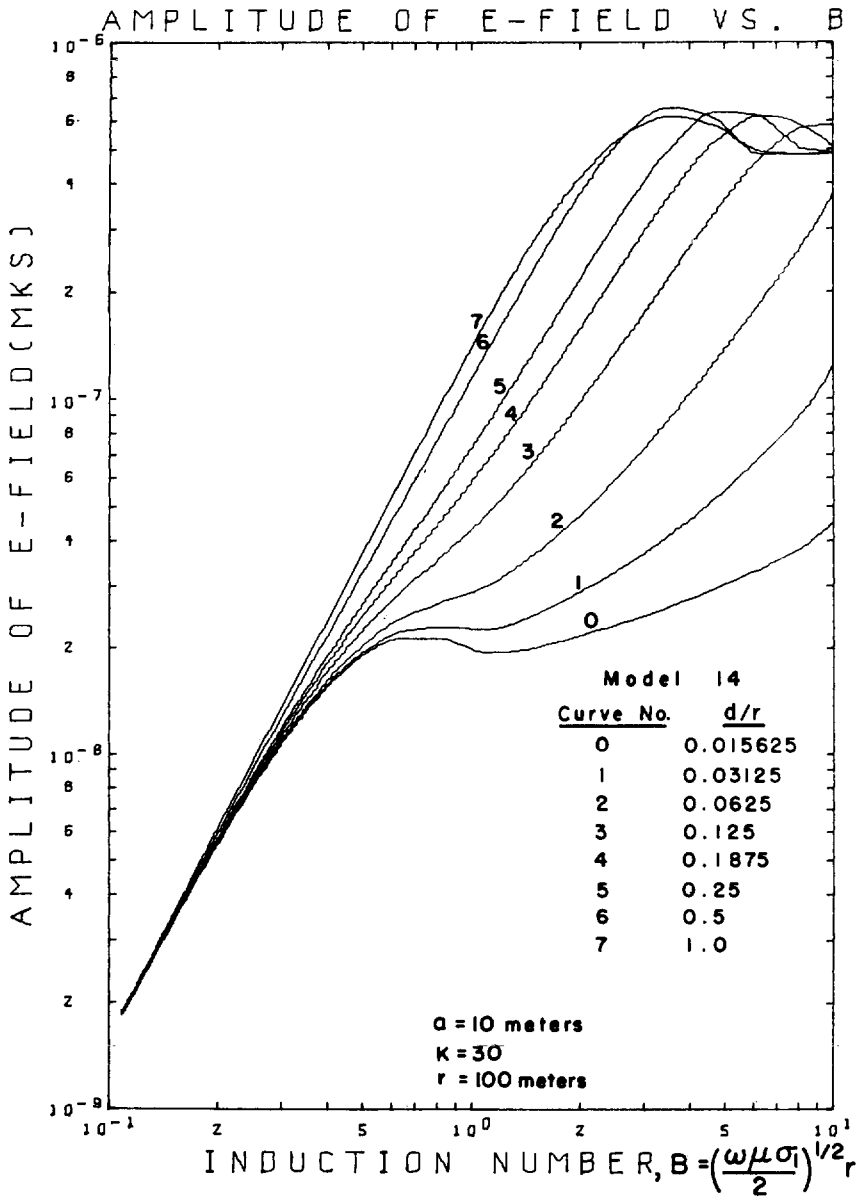

FIG. 3. Amplitude of E field versus induction number for Model 14, parametric sounding.

as Model 14, is described by the following parameters:

Model 14: Two-layer model for parametric sounding.

$a = 10$ m, a is the radius of the loop.

$r = 100$ m, r is the distance between the center of the loop and the point of observation.

$\sigma_1 = 10^{-2}$ mhos/m, σ_1 is the conductivity of the top layer.

$\sigma_2 = 3 \times 10^{-1}$ mhos/m, σ_2 is the conductivity of the bottom layer.

$K = \sigma_2/\sigma_1 = 30$.

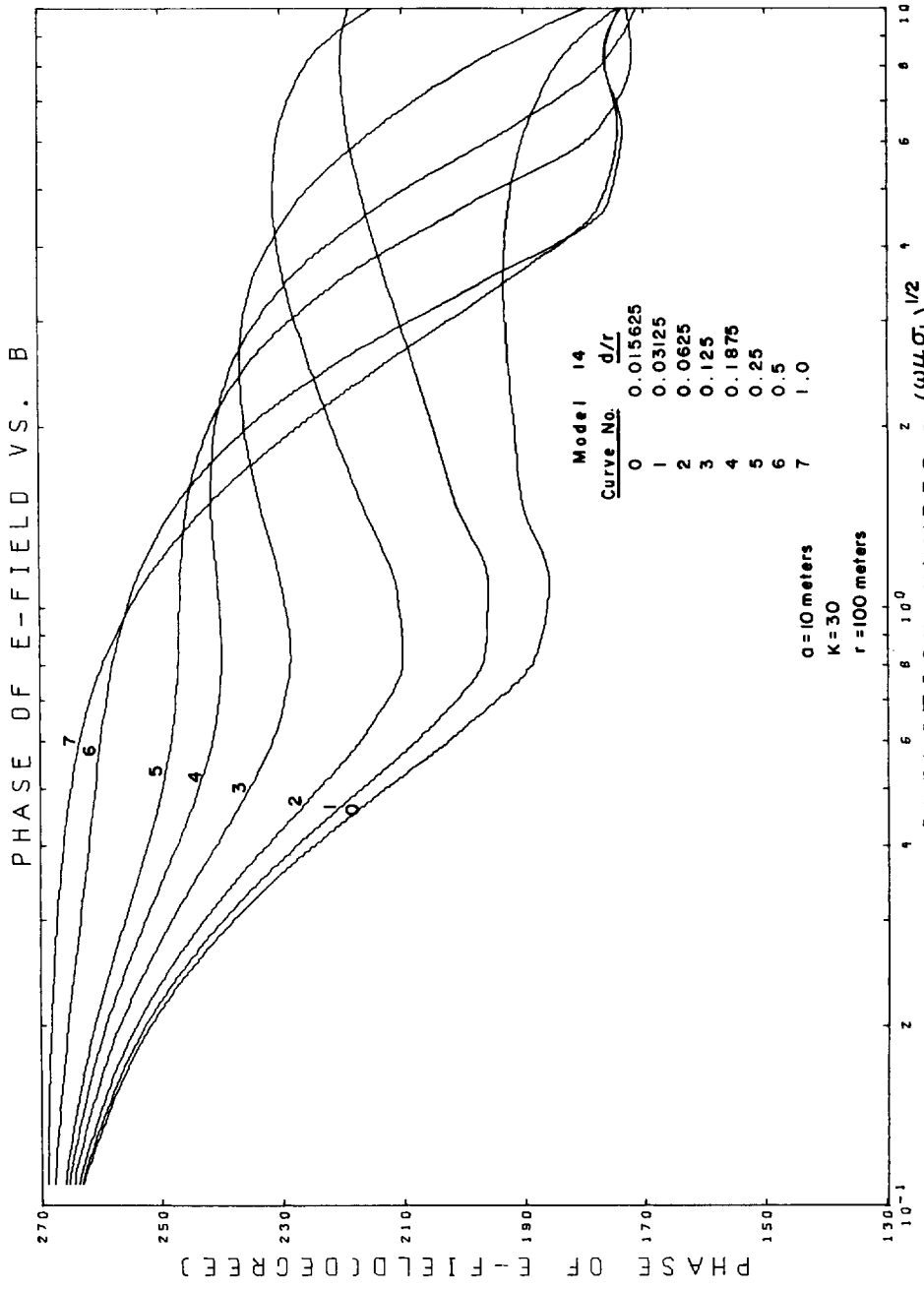

FIG. 4. Phase of E field versus induction number for Model 14, parametric sounding.

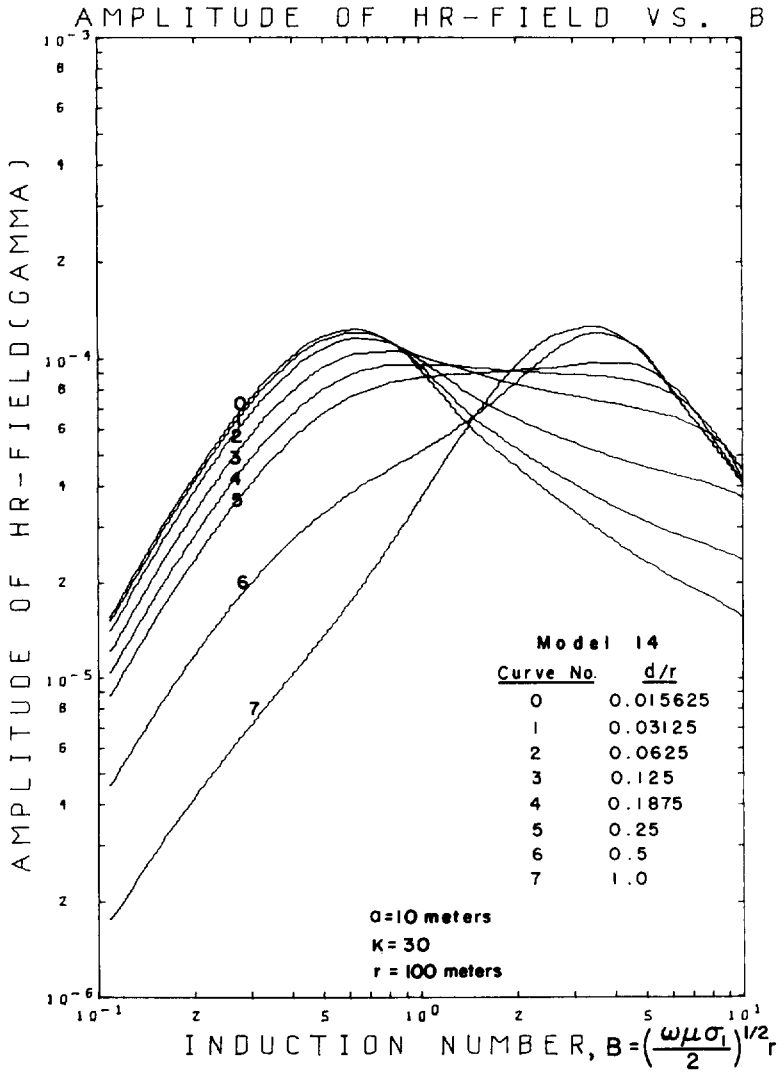

FIG. 5. Amplitude of H_r field versus induction number for Model 14, parametric sounding.

The responses for the 10 field quantities are plotted against the induction number B in Figures 3 through 12. Since interpretation can be made in terms of the dimensionless quantity d/r, where d is the thickness of the top layer and r is the source-detector separation, each figure contains eight curves corresponding to d/r ratios of 0.015625, 0.03125, 0.0625, 0.125, 0.1875, 0.25, 0.5, and 1.0.

The resolution of induction depth sounding depends largely upon the degree of dissimilarity in the theoretically computed response curves. The response curves for the moduli and the phases of field components shown in Figures 3 through 8 highlight good resolution. For this particular earth model, measurements of the above quantities, intended to deduce the depth to an electrical discontinuity, should be made at induction numbers greater than 0.5. The phase curves seem to be more diagnostic of structure than are the modulus curves. Dissimilarities are lost between the response curves 6 and 7 cor-

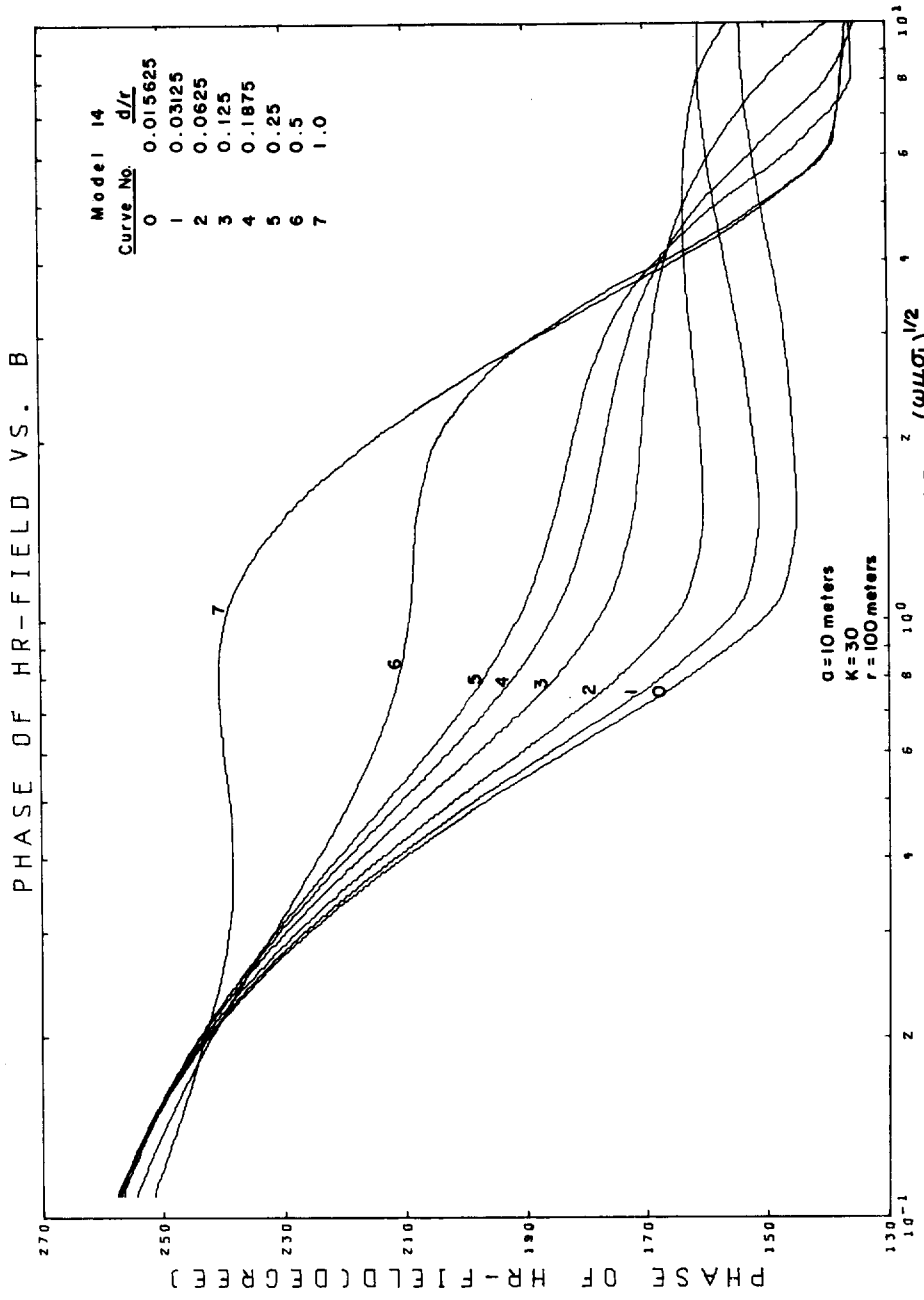

FIG. 6. Phase of H_r field versus induction number for Model 14, parametric sounding.

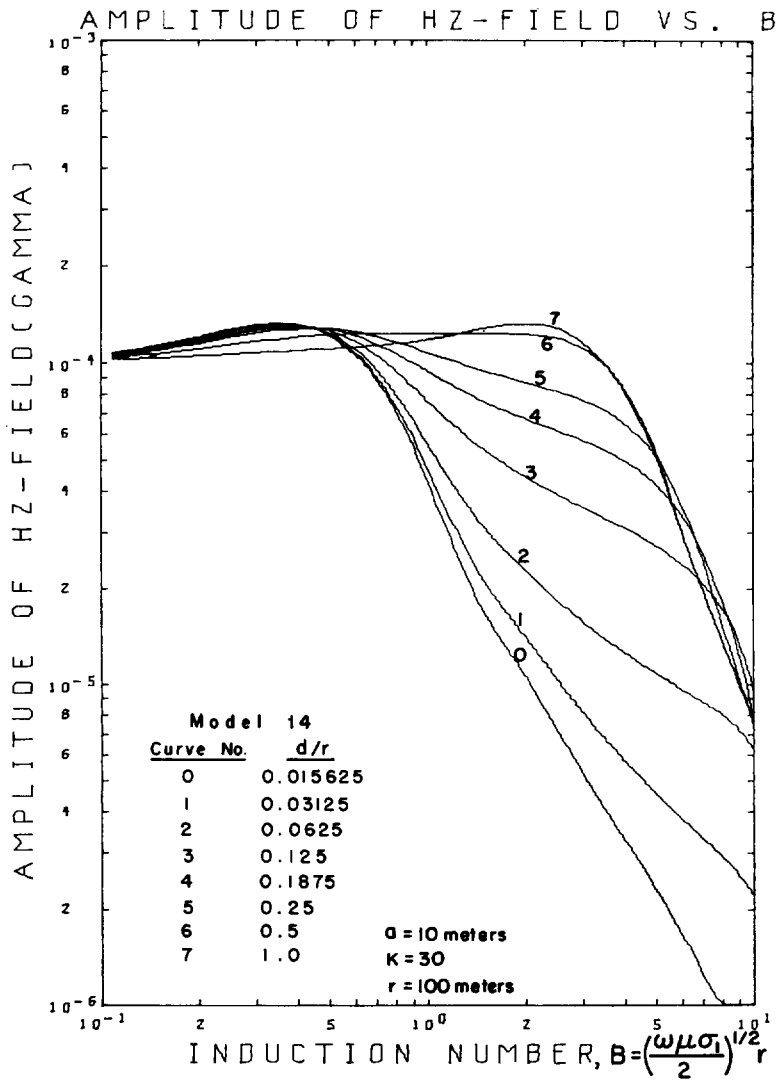

FIG. 7. Amplitude of H_z field versus induction number for Model 14, parametric sounding.

responding to d/r ratios of 0.5 and 1.0, respectively, in Figures 3, 4, 7, and 8. However, a most significant observation is that the modulus and the phase of the H_r field shown in Figures 5 and 6 still preserve a resolution between the response curves 6 and 7 over a low range of induction number, say $B<2.0$, permitting a depth of exploration greater than the source-detector separation.

The curves for polarization parameters given in Figures 9 through 12 are also well separated so that they are as indicative of layered structures as those for field components. However, the pattern is obscure for the phase of wave tilt shown in Figure 10. It can be seen from Figures 11 and 12 that the polarization ellipse is nearly linear with its major axis vertical at low frequencies and linear with its major axis horizontal at high frequencies, past a point of peak ellipticity. In particular, the ellipticity responses reveal a high resolution and may permit a depth of exploration greater than the source-detector separation over a proper range of induction number. It appears that the tilt angle and the ellipticity are the most

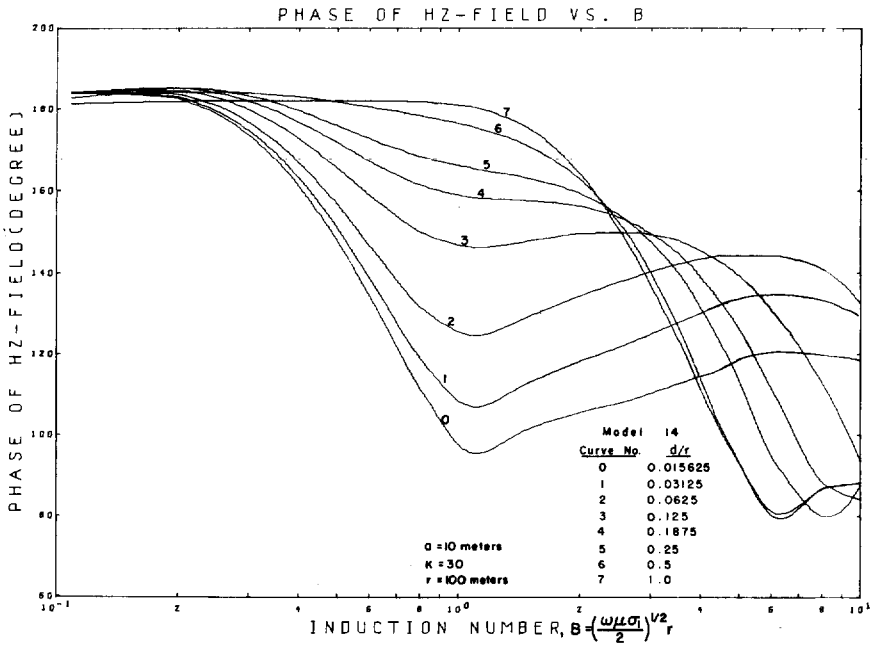

FIG. 8. Phase of H_z field versus induction number for Model 14, parametric sounding.

useful quantities among those to be measured for this type of electromagnetic sounding. They seem to be as diagnostic as other quantities and are easier and faster to measure in the field. Hence, subsequent discussion will be made in terms of the responses for tilt angle and ellipticity.

Since the radius of the loop is contained in the argument of one of the Bessel functions in the equations (12), (13), and (14), the field components should be affected by the size of the transmitting loop. Figures 13 and 14 show the effect of the loop size on the responses for tilt angle and ellipticity, respectively. In this model, the distance between the center of the transmitting loop and the point of observation is fixed at 3000 m. With σ_1 equal to 10^{-3} mhos/m, the operating frequency varies such that the induction number falls over the range between 0.1 and 10. Three cases are considered; i.e., a homogeneous half-space and two two-layered earth models with the thickness of the top layer being 375 m and 750 m corresponding to d/r ratios of 1:8 and 1:4, respectively. For two-layered models, the conductivity ratio $K(=\sigma_2/\sigma_1)$ is assumed to be 30. In Figures 13 and 14, the responses with a loop radius of 10 m are indicated by the solid line and those with the loop radius of 1000 m, by the dashed line. Significant differences in the response curves for both tilt angle and ellipticity in all cases are obvious. In general, it is necessary to make separate computations with the complete loop solution whenever the ratio r/a is less than 5.

Parametric sounding, conductivity decreasing with depth. The conductivity contrast of the two layers obviously plays a major role in their combined electromagnetic response. In the models considered above, the ground conductivity increases with depth ($K=30$) with the result that a high resolution of the layered structure was observed. Figures 15 and 16 illustrate the results for a model in which conductivity decreases with depth ($K=0.3$). The tilt angle and the ellipticity are plotted versus induction number in Figures 15 and 16, respectively. As expected, the individual curves do not exhibit the marked dissimilarity of the previous case, although the ellipticity still preserves some resolution over a range of high induction numbers, say $B>2.0$.

Geometric sounding, conductivity increasing with depth. Model D-14, used in computations for geometric sounding, has the same physical parameters as those of Model 14. The source

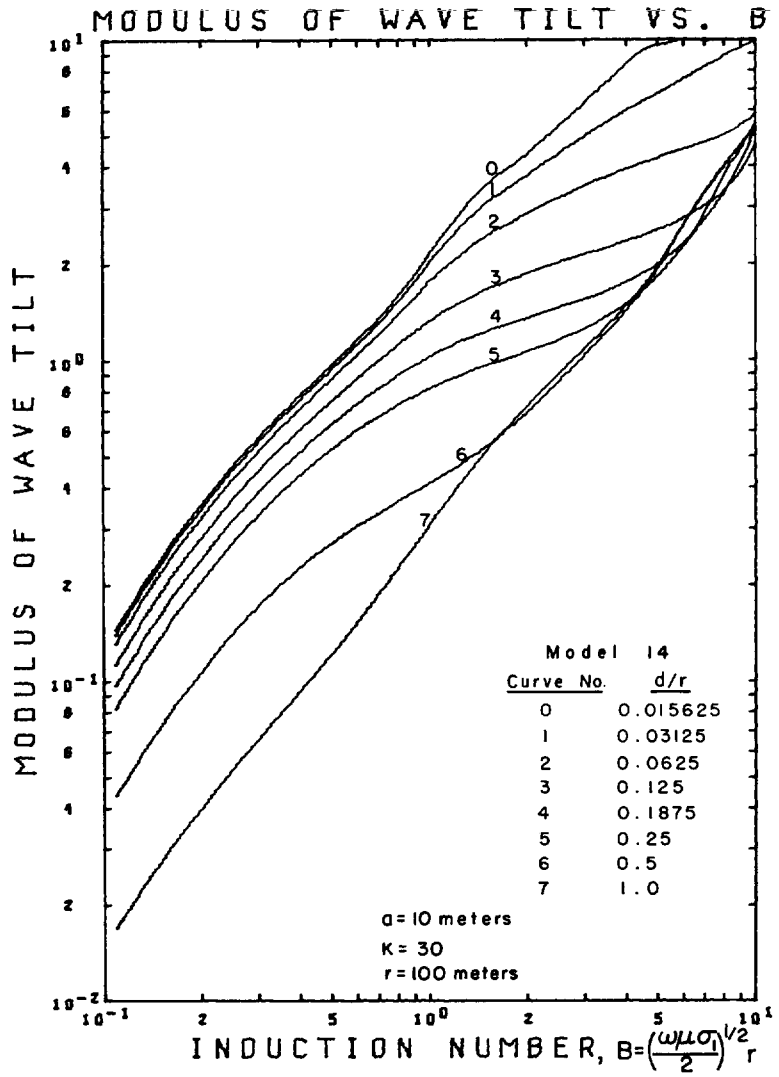

FIG. 9. Modulus of wave tilt versus induction number for Model 14, parametric sounding.

frequency is fixed at 500 hz and the source-detector separation r varies such that the induction number lies betwen 0.1 and 10. Figures 17 and 18 show the responses for the tilt angle and the ellipticity of Model D-14 for geometric sounding. Since the geometric sounding measurements can be interpreted in terms of a dimensionless parameter $D=2d/\delta_s$, where $\delta_s=(2/\omega\mu\sigma_1)^{1/2}$ is the skin depth computed with the conductivity of the top layer, both figures contain 7 curves, corresponding to the parameter D of 0.05, 0.1, 0.2, 0.4, 0.6, 0.8, and 1.2. In Figure 17, the curve shapes are almost identical and they shift toward the higher induction numbers as the electrical discontinuity becomes deeper, giving rise to difficulty in data interpretation without a prior knowledge of the conductivity of the top layer. However, the curves for the ellipticity in Figure 18 still highlight good resolution. In particular, the shape dissimilarity between curves 6 and 7

(*Text continued on page 884*)

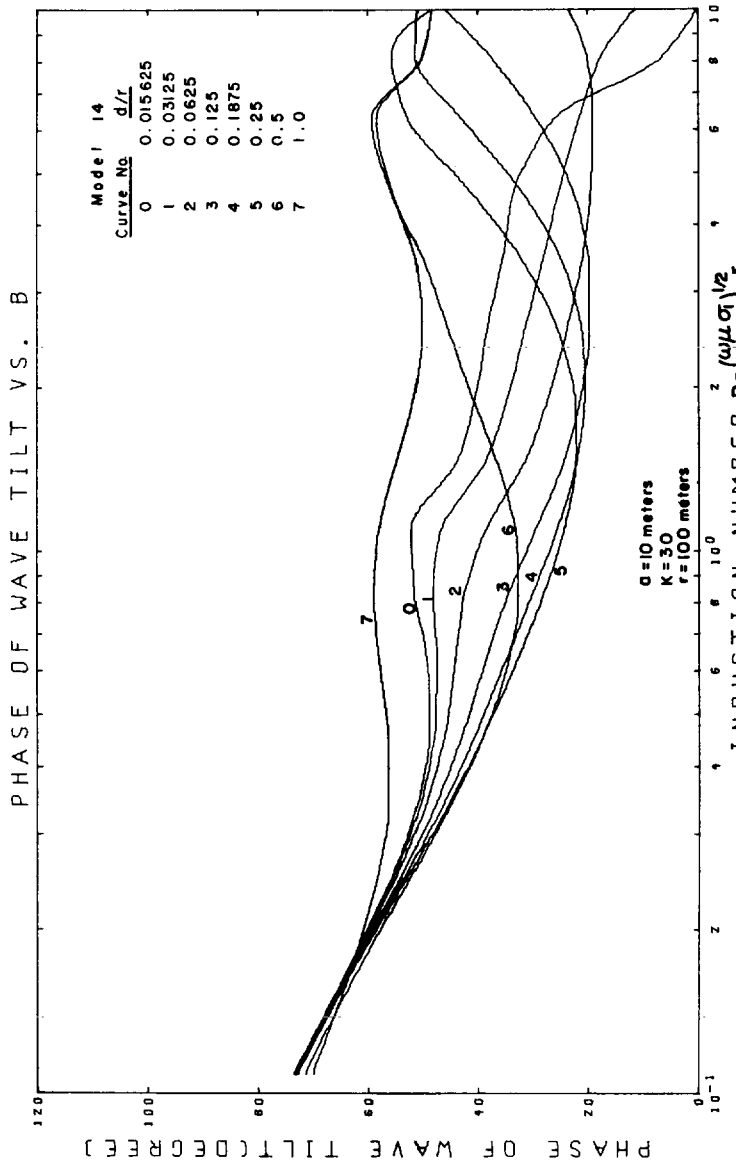

FIG. 10. Phase of wave tilt versus induction number for Model 14, parametric sounding.

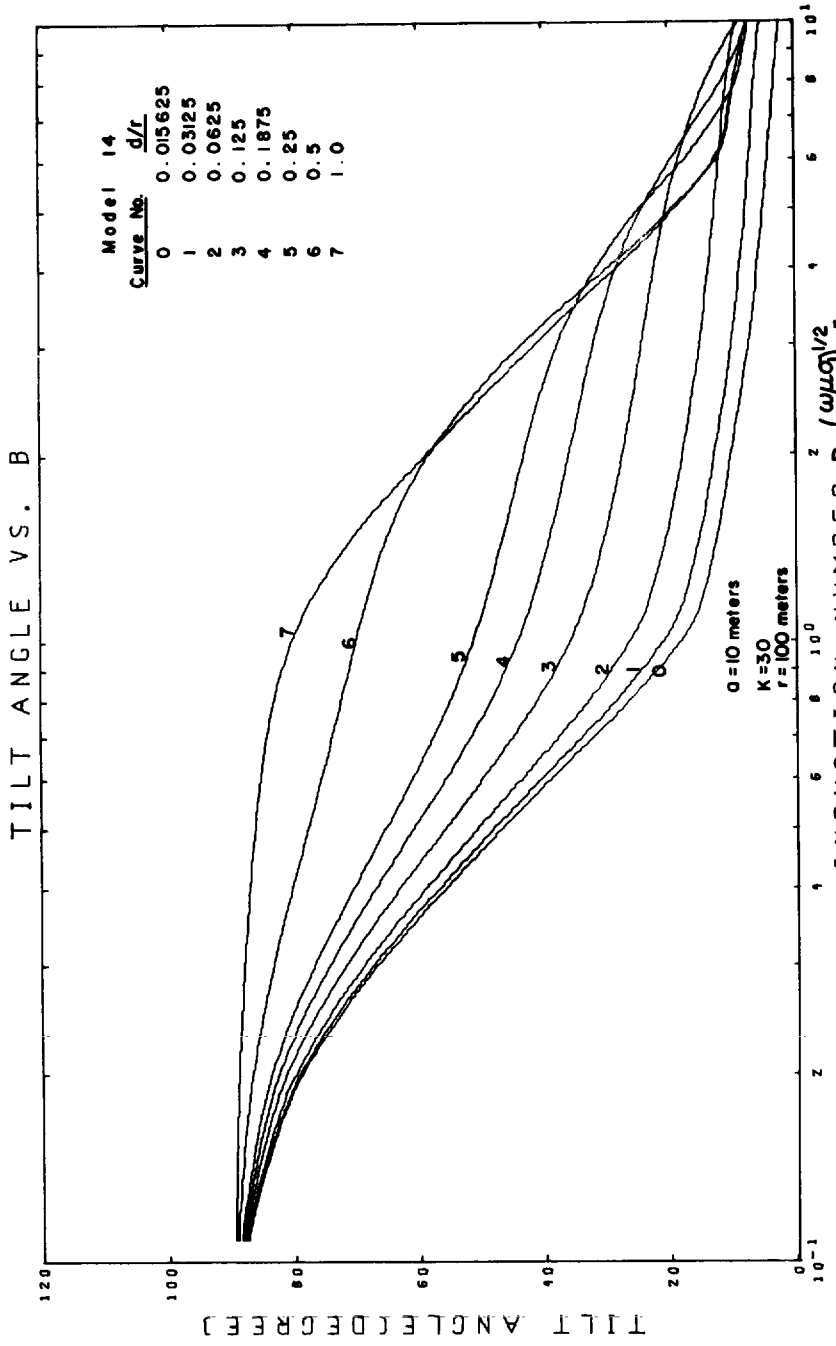

FIG. 11. Tilt angle versus induction number for Model 14, parametric sounding.

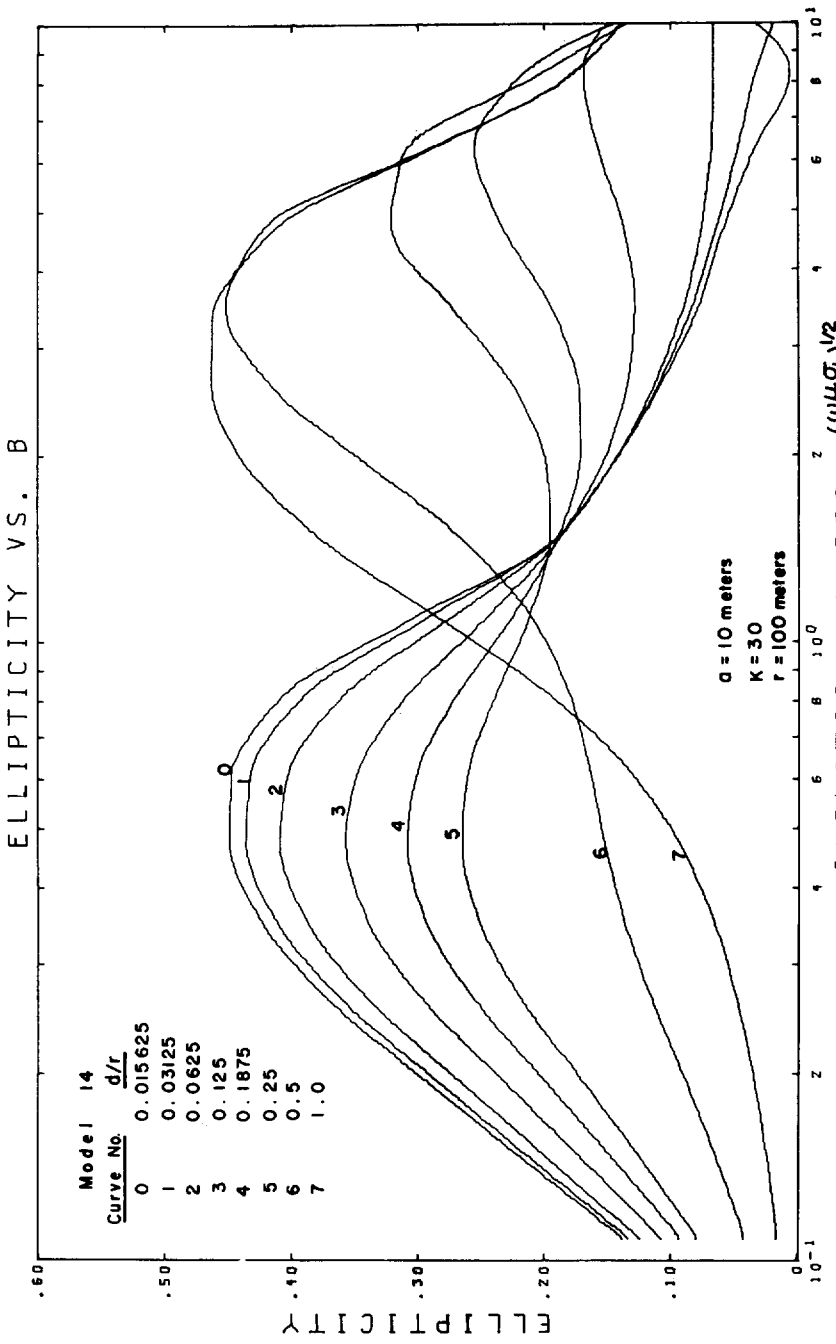

FIG. 12. Ellipticity versus induction number for Model 14, parametric sounding.

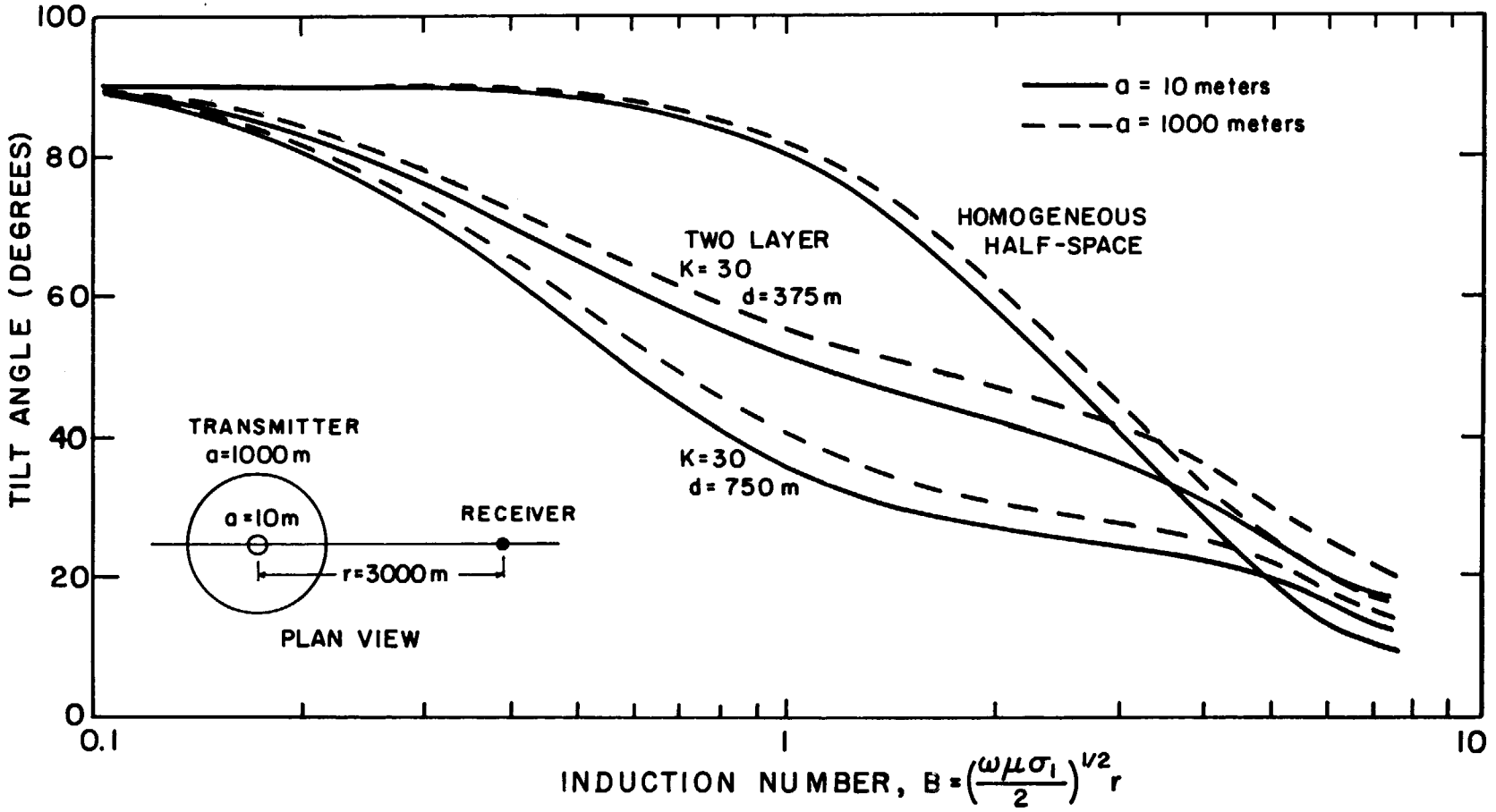

FIG. 13. Effect of loop size on tilt angle with parametric sounding.

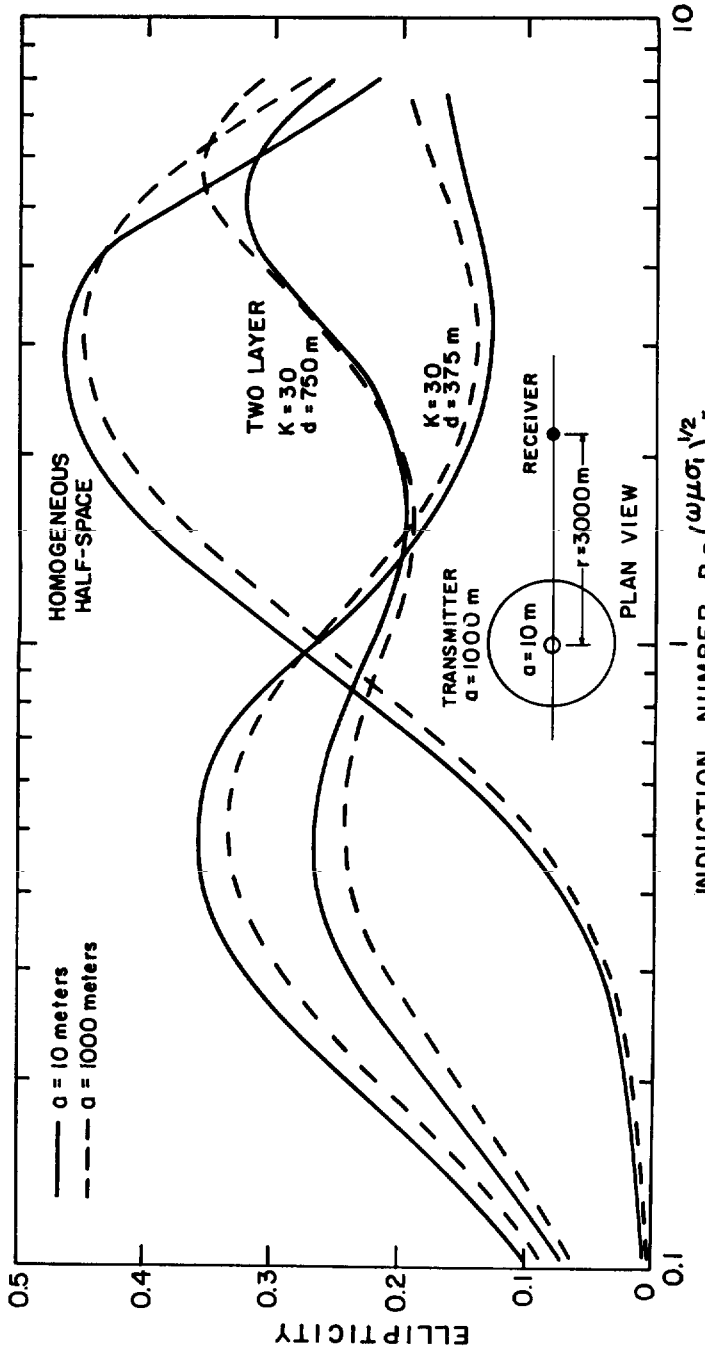

FIG. 14. Effect of loop size on ellipticity with parametric sounding.

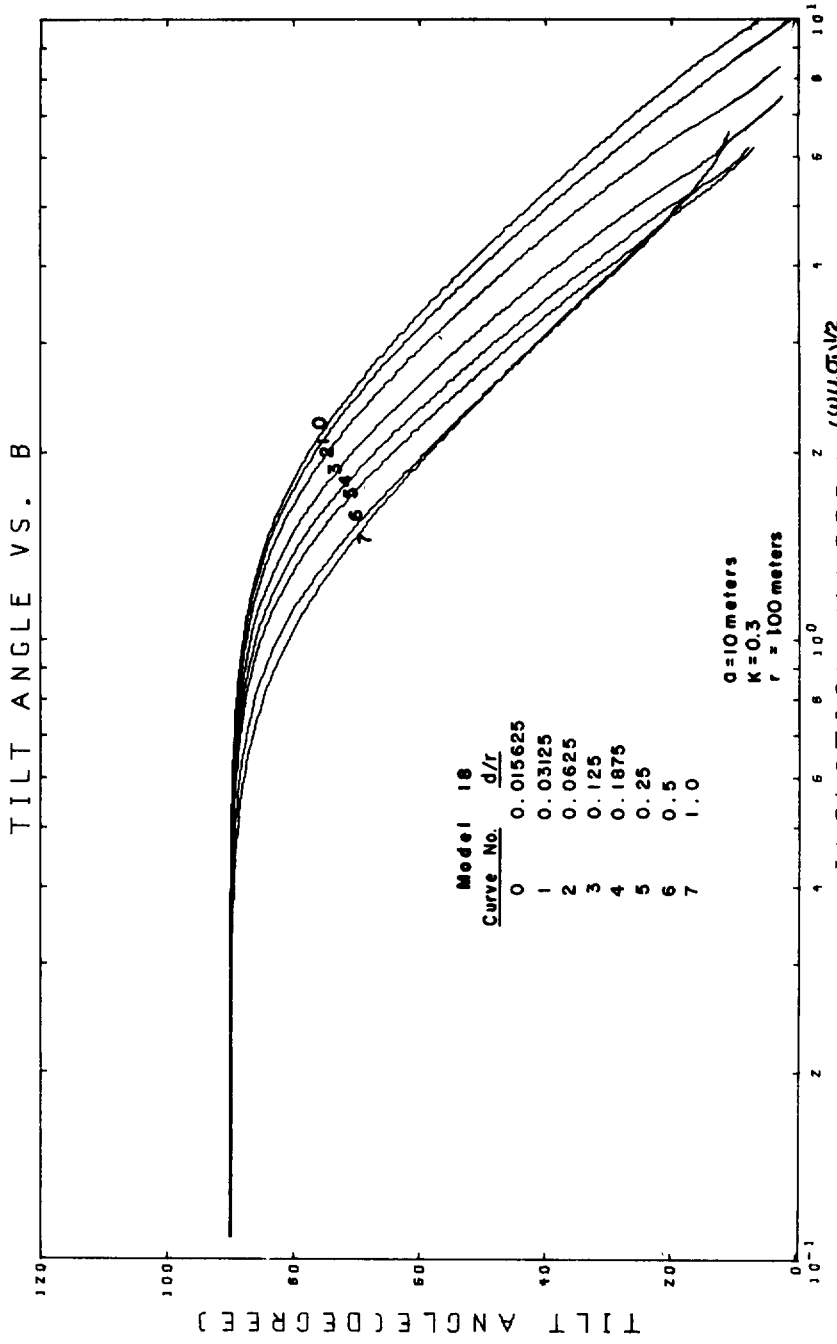

FIG. 15. Tilt angle versus induction number for Model 18, parametric sounding.

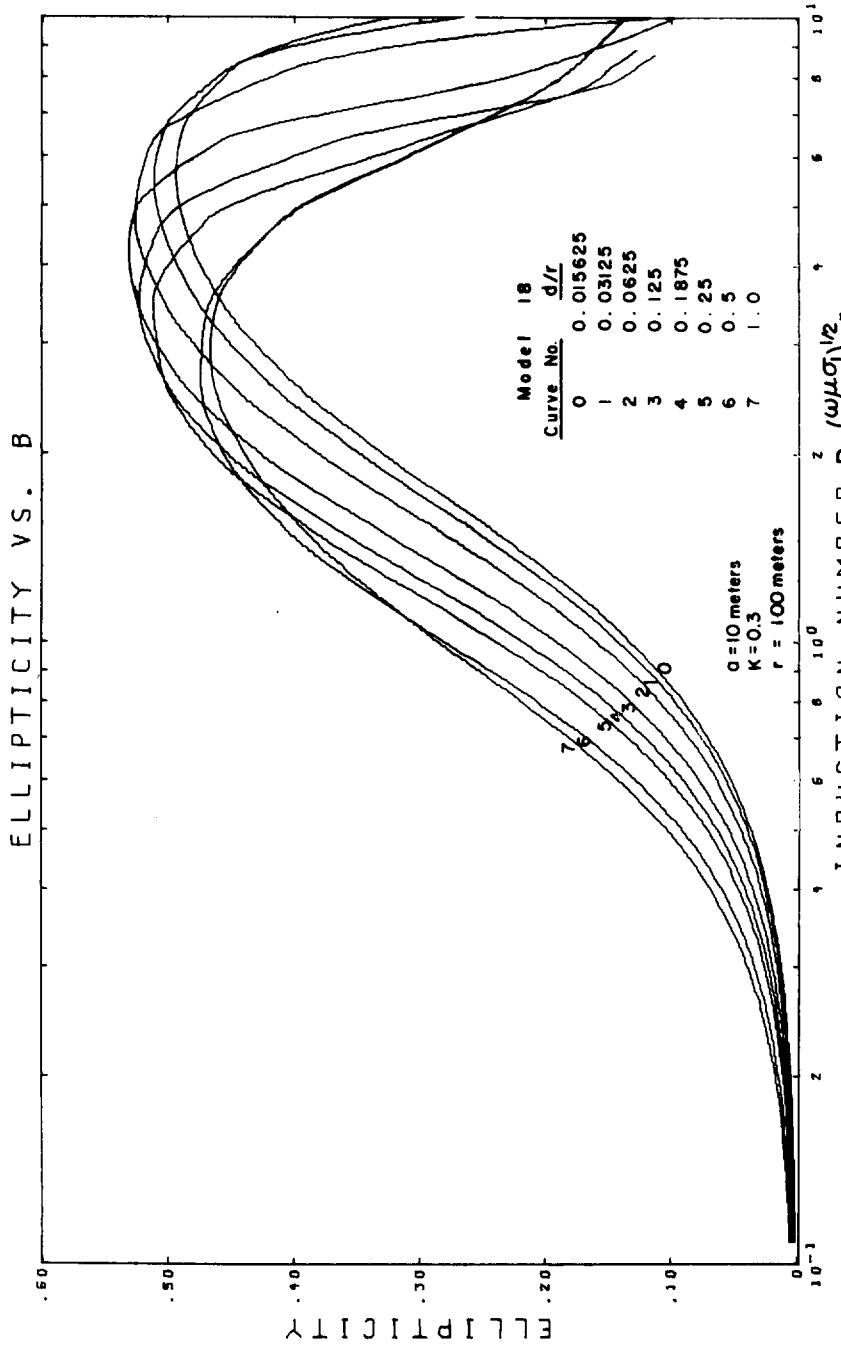

FIG. 16. Ellipticity versus induction number for Model 18, parametric sounding.

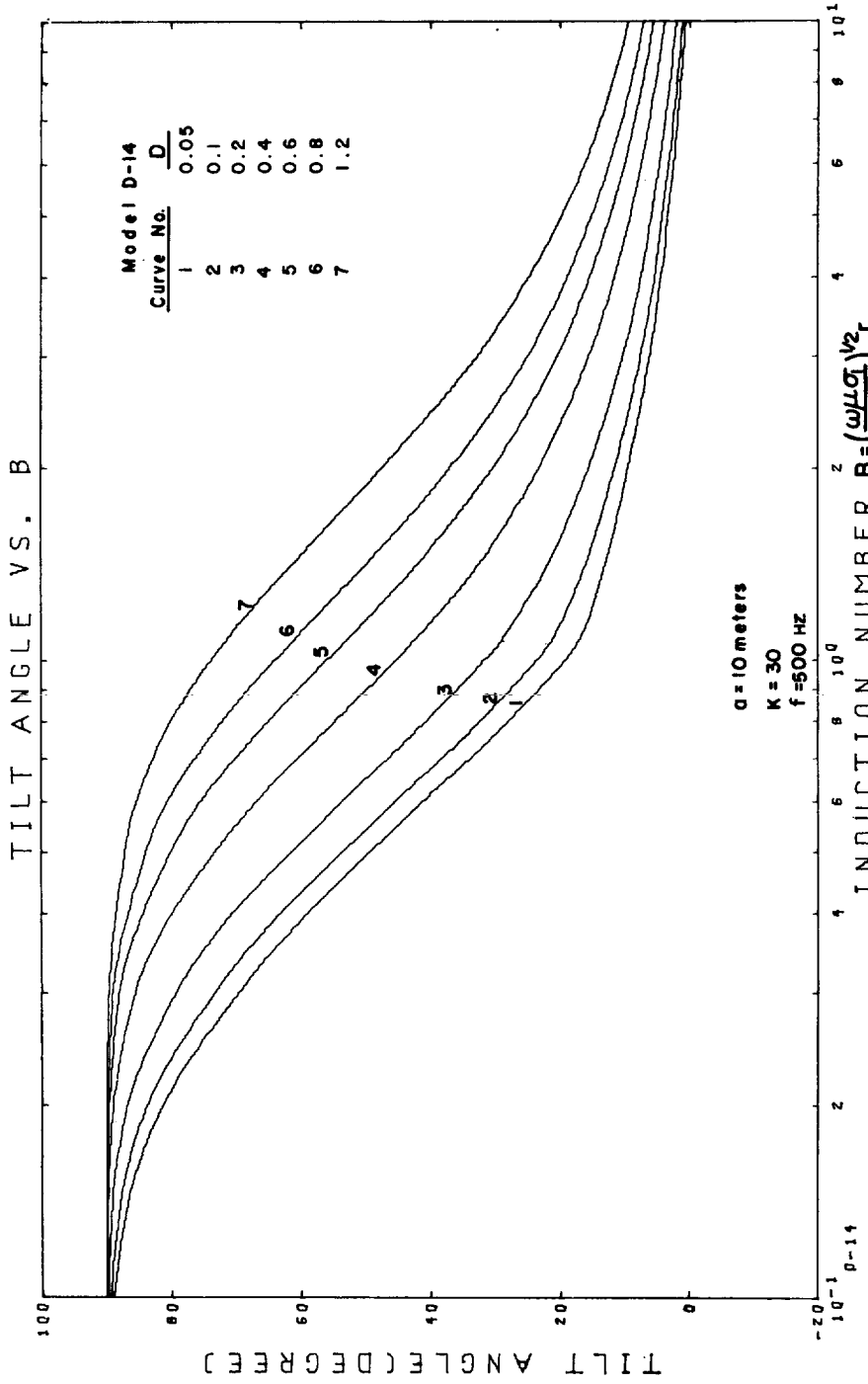

FIG. 17. Tilt angle versus induction number for Model D-14, geometric sounding.

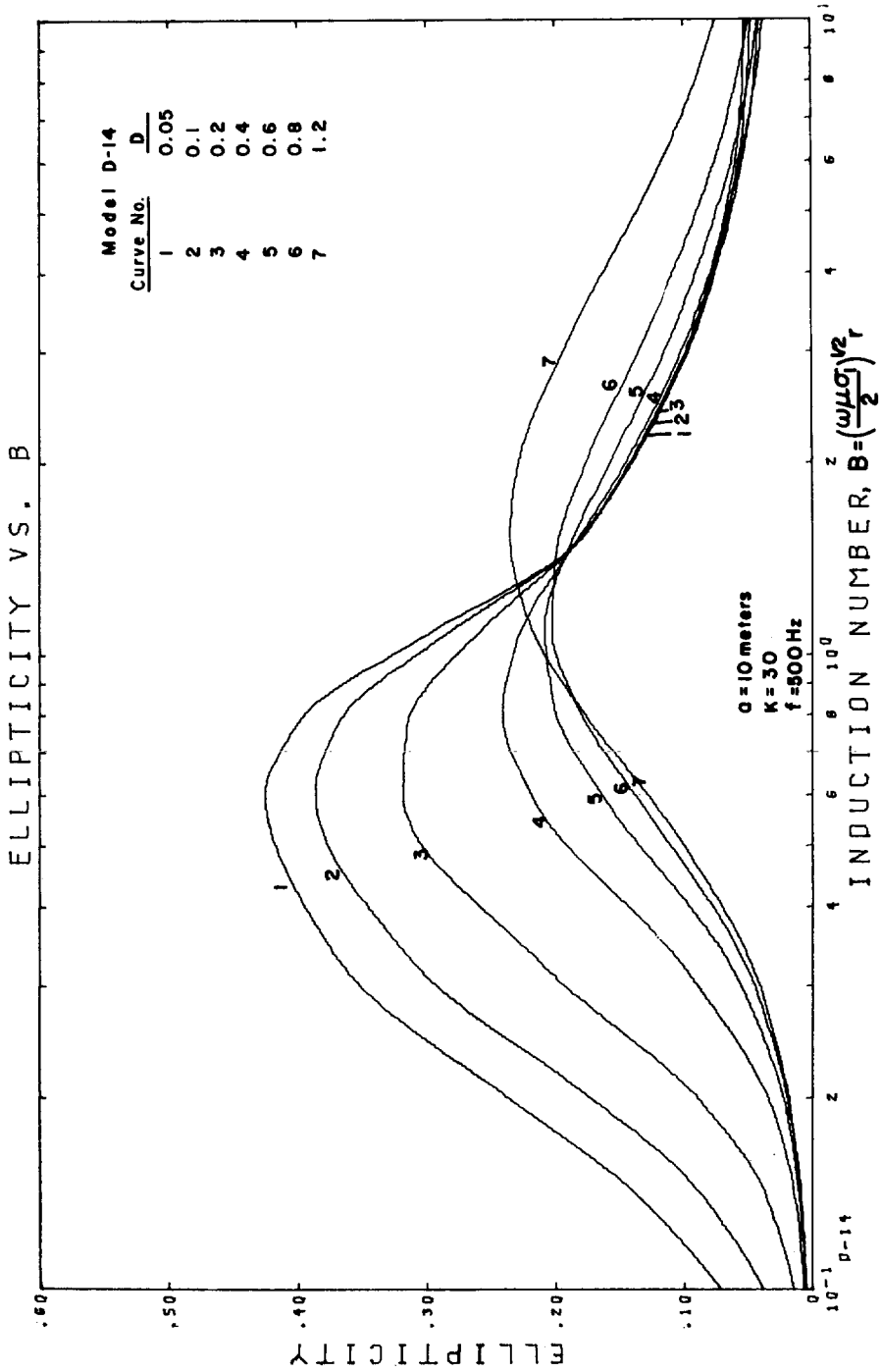

FIG. 18. Ellipticity versus induction number for Model D-14, geometric sounding.

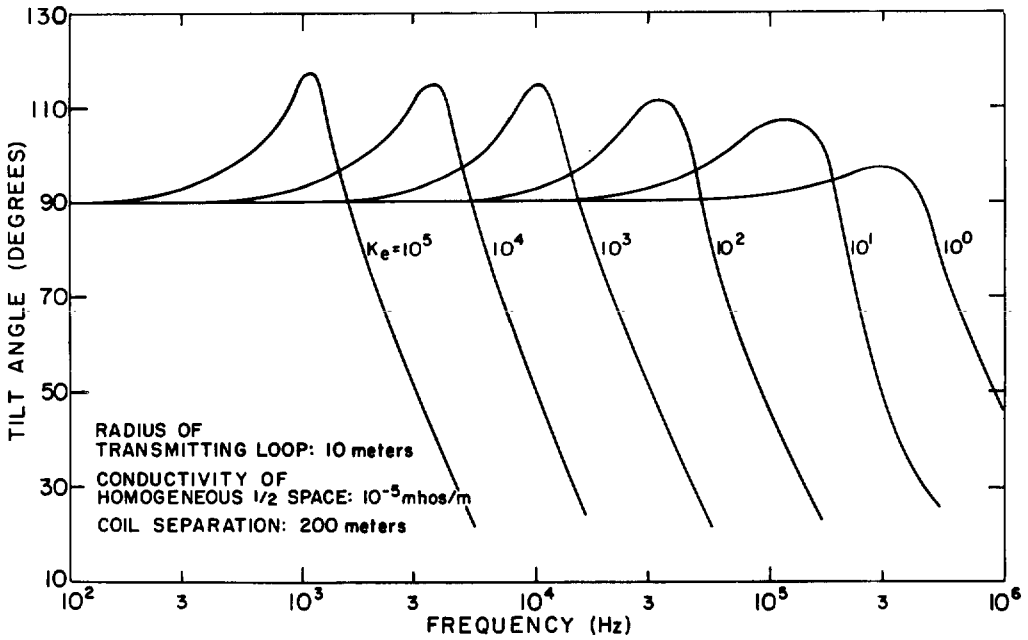

FIG. 19. Tilt angle response over homogeneous half-space with varying K_e values.

can be noticed at high induction numbers, say $B>0.8$, permitting a depth of exploration greater than $D=1$.

Measurement of dielectric constant for a homogeneous earth. In the above earth models, the conduction current far predominates over the displacement current, so that the quasi-static approximation with the neglect of displacement current is quite acceptable. For models in which $\tan\delta<1$, the displacement current predominates over the conduction current, so that the complete (*nonquasi-static*) solutions are required for the theoretical computations of field components. A model of a homogeneous half-space with a conductivity of 10^{-5} mhos/m is chosen, in which the radius of the transmitting loop and the source-detector separation are assumed to be 10 m and 200 m, respectively. The free space value of magnetic permeability is used. The relative dielectric permittivity K_e varies from 1 to 10^5. For simplicity, we assume that both conductivity and dielectric permittivity are independent of frequency, which is not generally true in nature. Figure 19 shows the tilt angle response plotted against frequency for various values of relative dielectric permittivity. For models such as this with $\tan\delta<1$, the neglect of displacement current is invalid. The geological environments in which such curves might apply include the moon and glaciers or deserts on earth.

Central induction sounding

We have chosen two simple two-layered models to illustrate the applicability of this loop current system to ground water exploration and possibly to petroleum exploration. Model 1 is described by the following paameters:

Models 1a and 1b

Layer 1

$$\sigma_1 = 10^{-2}\ \text{mhos/m, thickness } d \text{ meters}$$
$$\text{where } 5 \leq d \leq 30.$$

Layer 2

a. $\sigma_2 = 3 \times 10^{-1}$ mhos/m, thickness ∞,

$$K = \frac{\sigma_2}{\sigma_1} = 30.$$

b. $\sigma_2 = 3 \times 10^{-4}$ mhos/m, thickness ∞,

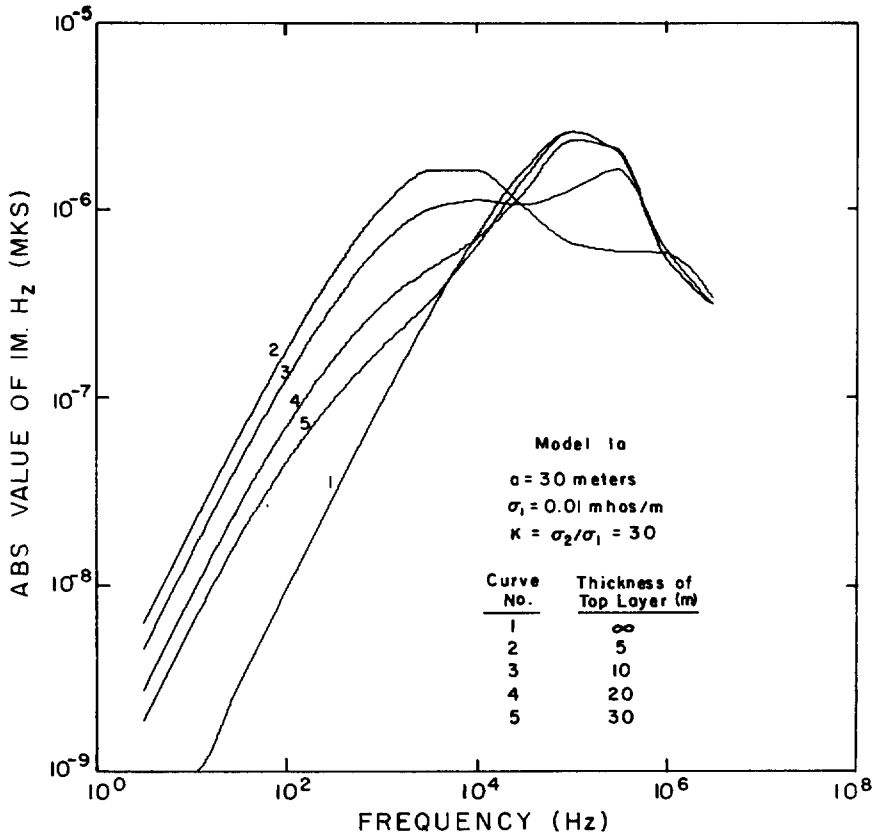

FIG. 20. Quadrature part of H_z versus frequency for Model 1a, central induction sounding.

$$K = \frac{\sigma_2}{\sigma_1} = 0.03.$$

In Models 1a and 1b, the radius of the transmitting loop is chosen to be 30 m. For Model 2 the physical parameters are the same as those in Model 1a but the radius of the transmitting loop is increased to 1000 m. In the following computations, the displacement terms will be included and free space values of ϵ and μ are used.

Since the field measurement by central induction sounding in the absence of any lateral inhomogeneity is confined to the vertical component of magnetic field (H_z), Figures 20 to 28 graph the quadrature part of H_z, the modulus of H_z, and the phase of H_z against frequency for the above models. With K set equal to 30 as in Model 1a, conductivity increases with depth and the curves for all three measurable quantities show that subsurface layering is easily resolved, as Figures 20, 21, and 22 reveal. We note from Figures 20 and 26 that the curves for the quadrature part of H_z versus frequency for Model 1a and Model 2 also indicate a good resolution of subsurface layering, even though the top layer thickness is as large as the radius of the transmitting loop. However, resolution is hardly noticeable in Figures 23, 24, and 25 for Model 1b, in which $K=0.03$, i.e., conductivity decreases with depth. It is suggested that the quadrature part should be measured over a wide range of frequency for this system for two reasons: 1) the quadrature part has a wide range of variation over a given frequency band in comparison with the variation of other quantities; and 2) a depth of exploration greater than the loop radius may be achieved by measuring the quadrature part. These characteristics are illustrated by the high degree of dissimilarity of curves 1 and 5 in Figures 20 and 26.

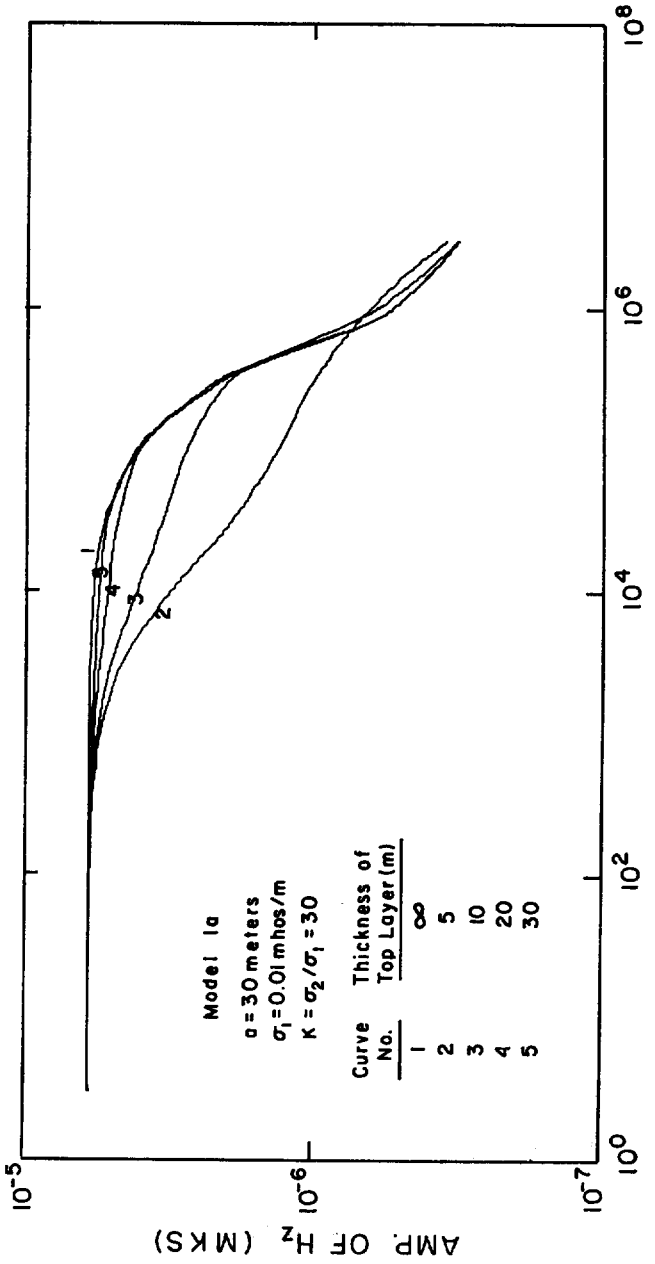

Fig. 21. Amplitude of H_z versus frequency for Model 1a, central induction sounding.

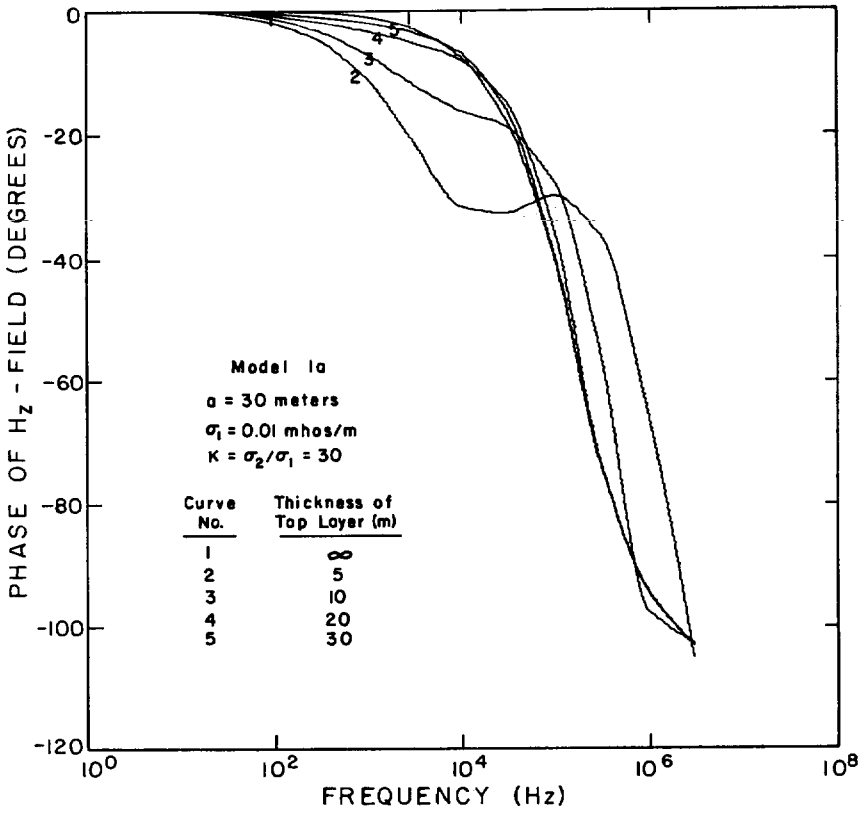

FIG. 22. Phase of H_z versus frequency for Model 1a, central induction sounding.

For these earth models, the vertical magnetic field may be computed with the neglect of displacement currents in both the air and the ground. For such cases, the theoretically computed responses can be plotted against the dimensionless induction number defined by $B = a/\delta_s$ where a is the loop radius and δ_s is the skin depth calculated with the conductivity of the top layer. This procedure considerably reduces the number of theoretical curves required for the interpretation of data. For central induction sounding over a layered earth model, the diagnostic range of response falls in the induction number range between 0.1 and 10.

Measurement of magnetic susceptibility of a homogeneous half-space

An interesting subsidiary application of the central induction method is the determination of magnetic susceptibility in situ and in the laboratory. The theoretical consideration behind this method is that the total magnetic field tends asymptotically toward a static value as frequency decreases, enabling us to determine the static magnetic permeability of a homogeneous half-space. It is important to note that low frequency fields should be used to avoid measurement of the earth's static field. Over a range of very low frequencies, magnetic induction dominates electrical conduction, whose effect becomes negligible. In addition, the effect of displacement current is entirely negligible. At low frequencies, the secondary quadrature part vanishes and only the total in-phase part is present. Figure 29 reveals the response of a homogeneous half-space with a loop radius of 3 cm for laboratory measurement and with a loop radius of 50 cm for measurement in situ. It should be noted in Figure 29 that the product of N and I in actual calculation varies according to the loop size in order to keep a unit magnetic moment of the loop. Since the responses are well separated over the range of

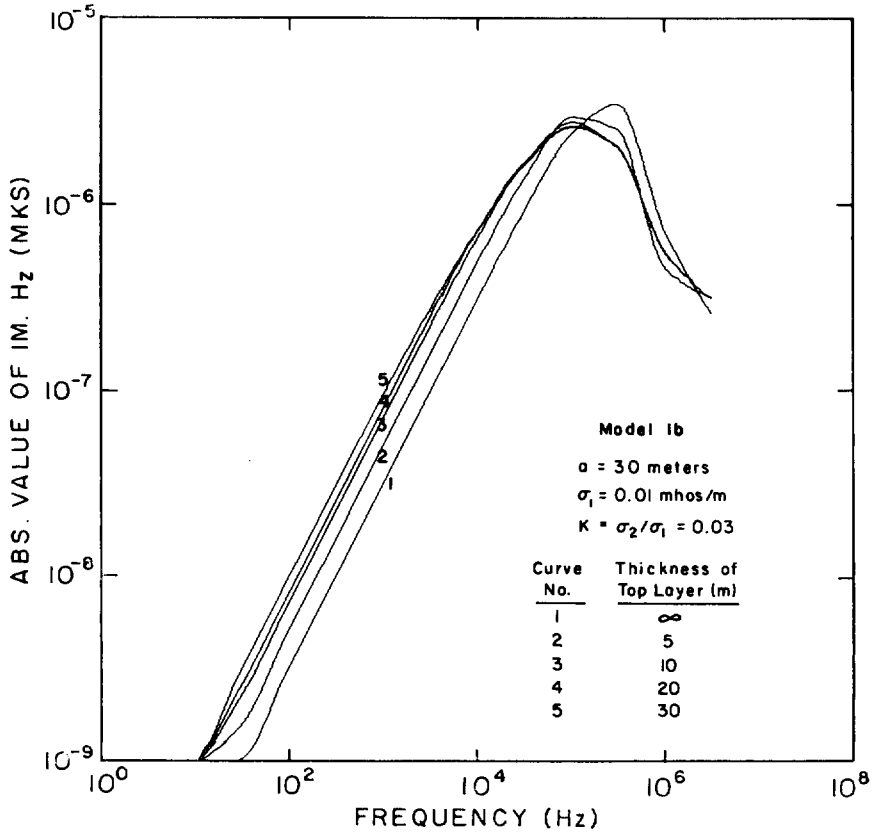

FIG. 23. Quadrature part of H_z versus frequency for Model 1b, central induction sounding.

magnetic permeability of interest, the magnetic permeability can be easily deduced. The magnetite content shown in Figure 29 was obtained from the curve given by Mooney and Bleifuss (1953). Practically, this method may be effective in distinguishing remanent from induced magnetic anomalies, rather than in regional susceptibility mapping.

The effect of a conductive half-space on calculation of the normal field in Turam exploration

A final application of our theoretical computation lies with the Turam method. Bosschart (1964 and 1968) advocates the use of a calculated free space vertical magnetic field from a loop source as a means of providing a normal correction when utilizing the Turam method. When measurements are made at two consecutive points m and $m+1$, the normal ratio of the primary field is written as H^p_m/H^p_{m+1} and the ratio observed in the presence of a secondary field as H^t_m/H^t_{m+1}, where the superscripts p and t refer to the primary field and the total field, respectively. Then the reduced ratio C is defined as

$$C = \frac{H^t_m}{H^p_m} \Big/ \frac{H^t_{m+1}}{H^p_{m+1}} .$$

Bosschart (1964) indicates that the normal ratios for an identical conductor at two different locations with respect to the loop are the same, provided that the direction of the primary flux is the same. This is the basis of the free-air correction on Turam data. However, the quantity C will depart from unity wherever the ground is conductive.

The observed normal ratio is not identical to the free space normal ratio if the effect of a uniform ground conductivity is taken into account. The effect of the ground conductivity is shown in

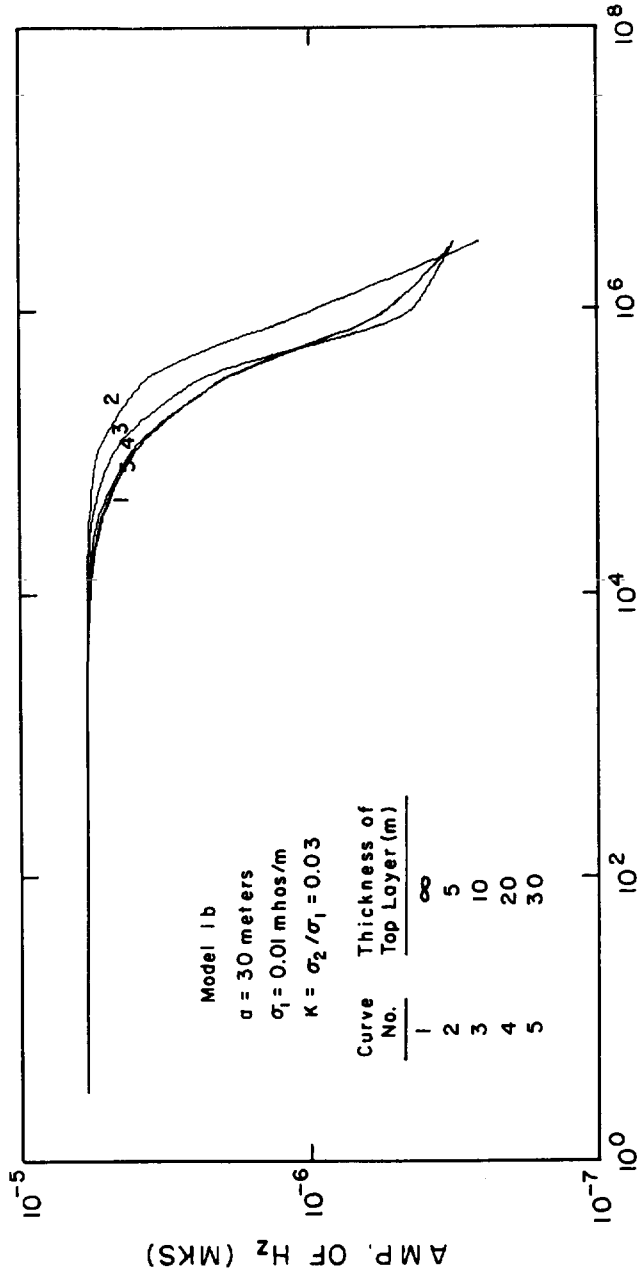

FIG. 24. Amplitude of H_z versus frequency for Model 1b, central induction sounding.

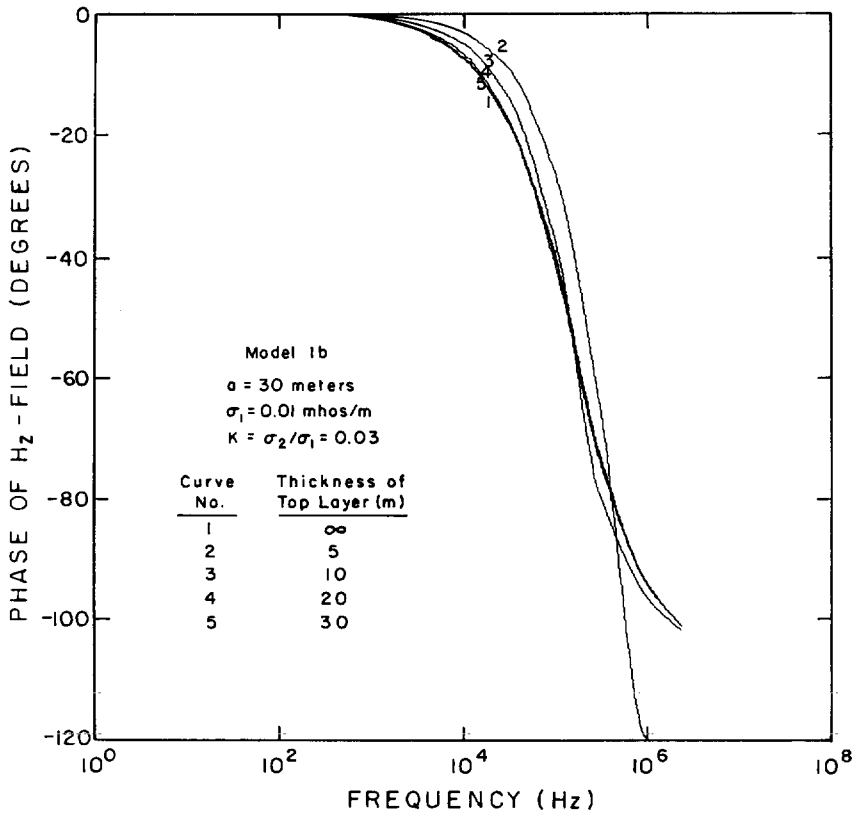

FIG. 25. Phase of H_z versus frequency for Model 1b, central induction sounding.

Figure 30, in which the moduli of the total magnetic fields at the point m, computed with equation (14), are plotted against the distance between the center of a transmitting loop and the central point of two detectors. The operating frequency is assumed to be 200 hz and the loop radius 1000 m. The curve for $\sigma=0$ represents the primary field in free space. The deviation of the curves for $\sigma=5\times10^{-3}$ mhos/m and $\sigma=10^{-2}$ mhos/m from the curve for the primary field becomes significant as the distance increases, say for r greater than 1600 m. This effect of the ground conductivity is more clearly shown in Figure 31. The deviation from unity of the reduced ratio increases as the distance increases, where the ground conductivity is greater than 10^{-3} mhos/m. This deviation also gives rise to difficulty in quantitatively separating the effects of local inhomogeneities from the effects of the homogeneous or mean layered earth. Further, the depth of the exploration is decreased as the mean apparent conductivity increases. Thus three factors —deviation from unity of the reduced ratio, difficulty in quantitative interpretation, and decreasing depth of exploration are expected to be important in the conduct of Turam surveys for a wide range of earth models as illustrated in Figures 30 and 31. In view of these results, caution should be exercised in interpreting Bosschart's (1968) assurance that Turam is superior to all other electromagnetic prospecting methods because of its freedom from topographic error, great depth of exploration, and facility for quantitative interpretation.

CONCLUSIONS

In the theoretical model studies presented for inductive depth sounding, a high resolution of subsurface electrical layering is observed in the sounding curves of field components as well as in the sounding curves of parameters of the magnetic polarization ellipse. For most earth layered struc-

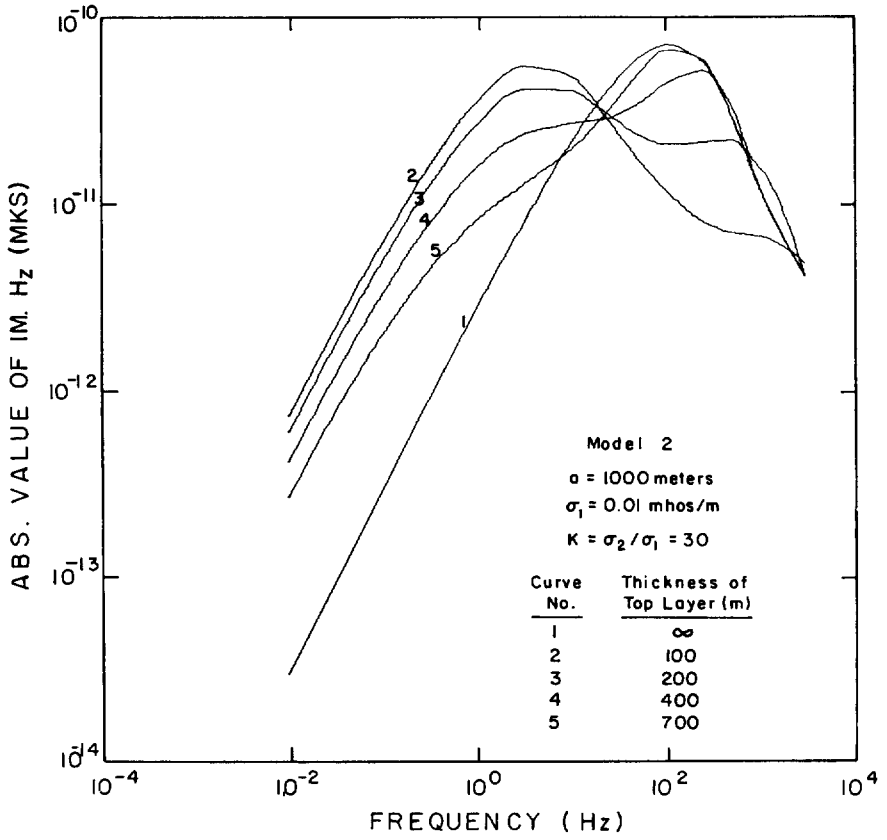

FIG. 26. Quadrature part of H_z versus frequency for Model 2, central induction sounding.

tures, measurements of field quantities should be made over a range of induction number $B=(\omega\mu\sigma_1/2)^{1/2}r$ between 0.1 and 10. It appears that the tilt angle and/or the ellipticity sounding system in either parametric or geometric mode is well suited to exploration for ground water and petroleum because of the simplicity and the speed of field measurements. For both modes, theoretical computations should be made with loop solutions instead of dipolar solutions. In addition, it has been demonstrated that there is a necessity for the complete loop solutions without quasi-static approximations in certain geologic environments where $\tan\delta<1$ and/or for certain source-detector geometrics.

Sounding can also be accomplished by measurement of the magnetic field as a function of the operating frequency at the center of a transmitting loop. In particular, the response for the quadrature part of vertical magnetic component shows good detection of an electrical discontinuity at a depth as large as the loop radius. The diagnostic response falls over a range of the induction number $B=(\omega\mu\sigma_1/2)^{1/2}a$ between 0.1 and 10. The limitation of this sounding system is that the responses reveal a good resolution only for the case of conductivity increasing with depth.

The feasibility of the determination of in-situ static magnetic permeability has been explored by use of the central induction measurements at low frequencies. The merit of the method arises in its ability to separate out the effect of the earth's static field.

Free-air correction for the reduction of Turam data is not valid where a surveyed area has a high ground conductivity, say $\sigma>10^{-3}$ mhos/m. The effect of the ground conductivity should be taken into account in the calculation of normal ratios with the complete loop solutions over a homogeneous or a mean layered earth model.

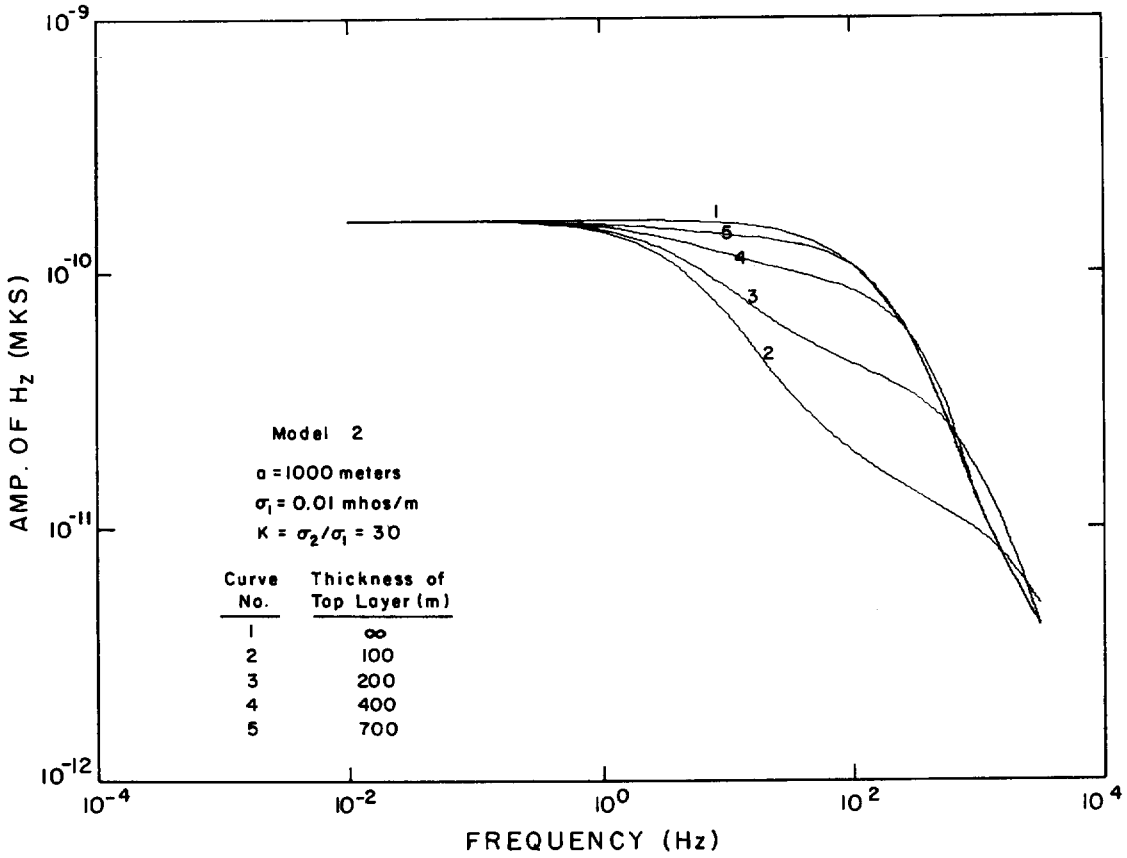

FIG. 27. Amplitude of H_z versus frequency for Model 2, central induction sounding.

ACKNOWLEDGMENTS

The work herein reported was sponsored by the Water Resources Center of the University of California (WRC Project W190) and by the Office of Water Resources Research, United States Department of the Interior, which provided "matching funds" under Public Law 88–79 (OWRR Project No. B-067-Cal).

APPENDIX A. NONLINEAR TRANSFORMATION (*G*-TRANSFORMATION)

Let f be a real-valued function of a real variable x such that f is continuous for $x\epsilon[a, \infty)$ and

$$F(t) = \int_a^t f(x)dx \to S \neq \pm \infty \quad \text{as } t \to \infty. \tag{A-1}$$

Also suppose there are, at most, countably many values of $x > a$ such that $f(x) = 0$.

Let us define

$$R(t; k) = \frac{f(t + k)}{f(t)} \quad \text{for } k > 0 \text{ and } f(t) \neq 0.$$

Further suppose that $R(t; k) \neq 1$ for t sufficiently large and that

$$\lim_{t \to \infty} R(t; k) = R(k).$$

Definition: if $R(t; k)$ exists $\neq 1$, then for $t \geq a$,

$$G[F; t, k] = \frac{F(t + k) - R(t; k)F(t)}{1 - R(t; k)}. \tag{A-2}$$

Theorem: If

(i) $f(t)$ alternates in sign as $t \to \infty$,

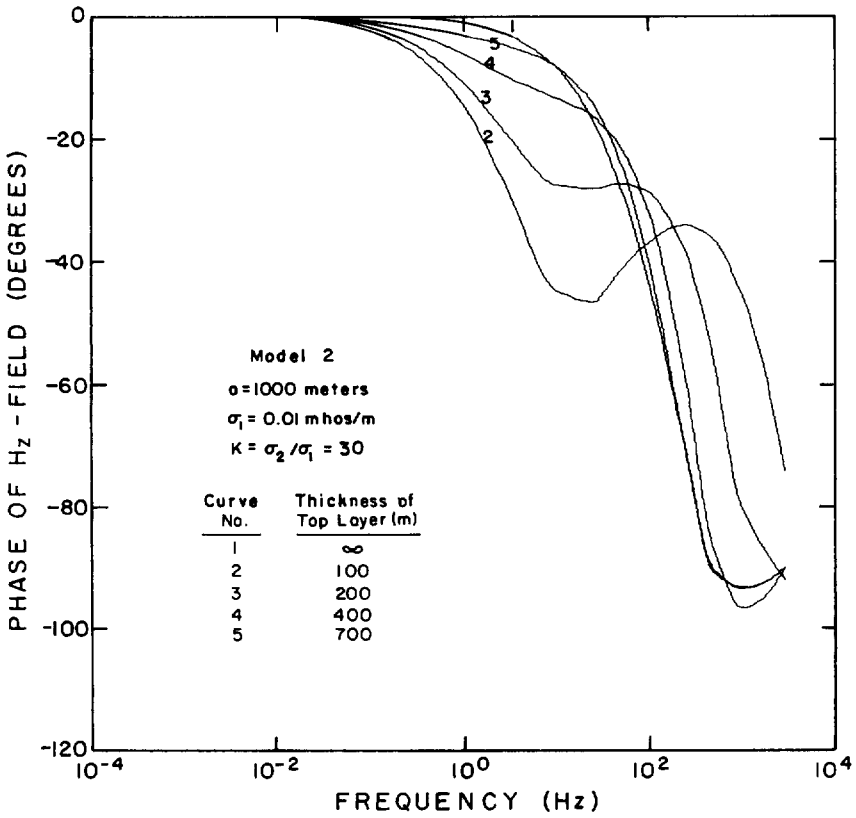

FIG. 28. Phase of H_z versus frequency for Model 2, central induction sounding.

(ii) the zeros of $f(t)$ for $t \geq t_1$ are given by $t_1 + pL$, where $p = 0, 1, 2, \ldots$ with $L > 0$,
(iii) $\lim_{t\to\infty} f(t)$ exists,
(iv) there exists $k \in (0, 1)$ such that $G[F; t, k]$ converges as $t \to \infty$, then $G[F; t, k] \to \infty$ as $t \to \infty$.

The proof of the theorem will not be given here. See the original paper by Gray and Atchison (1967).

Furthermore, equation (A-2) can be altered to

$$G[F; t, k] = \frac{F(t+k) - F(t)}{1 - R(t; k)} + F(t) = \frac{\int_t^{t+k} f(x)dx}{1 - R(t; k)} + \int_0^t f(x)dx. \quad \text{(A-3)}$$

Atchison and Gray (1968) introduced other types of nonlinear transformation for the case of $R(t; k) = 0$ or 1. However, $R(t; k) = 0$ or 1 does not occur in our problem. Hence, G-transformation was exclusively employed to improve the rate of convergence by use of equation (A-3).

REFERENCES

Atchison, T. A., and Gray, H. L., 1968, Nonlinear transformations related to the evaluation of improper integrals: II, SIAM. J. Numer. Analy., v. 5, p. 451–459.

Bhattacharyya, B. K., 1959, Electromagnetic fields of a transient magnetic dipole on the earth's surface: Geophysics, v. 14, p. 89–108.

——— 1963, Electromagnetic fields of a vertical magnetic dipole placed above the earth's surface: Geophysics, v. 28, p. 408–425.

Bosschart, R. A., 1964, Analytical interpretation of fixed source electromagnetic prospecting data: Delft, Waltman Publishing Co.

——— 1968, Ground EM prospecting: Mining in Canada, December, p. 13–19.

(*Continued on page 896*)

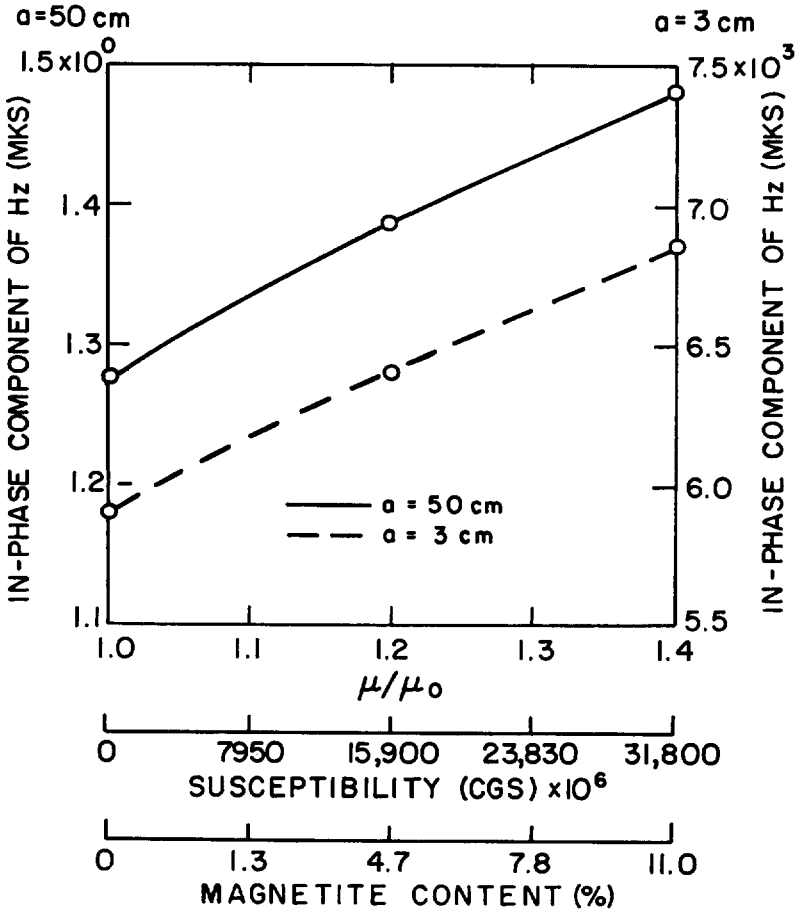

FIG. 29. In-phase H_z response of homogeneous, conductive magnetic half-space at low frequencies with varying magnetic permeability.

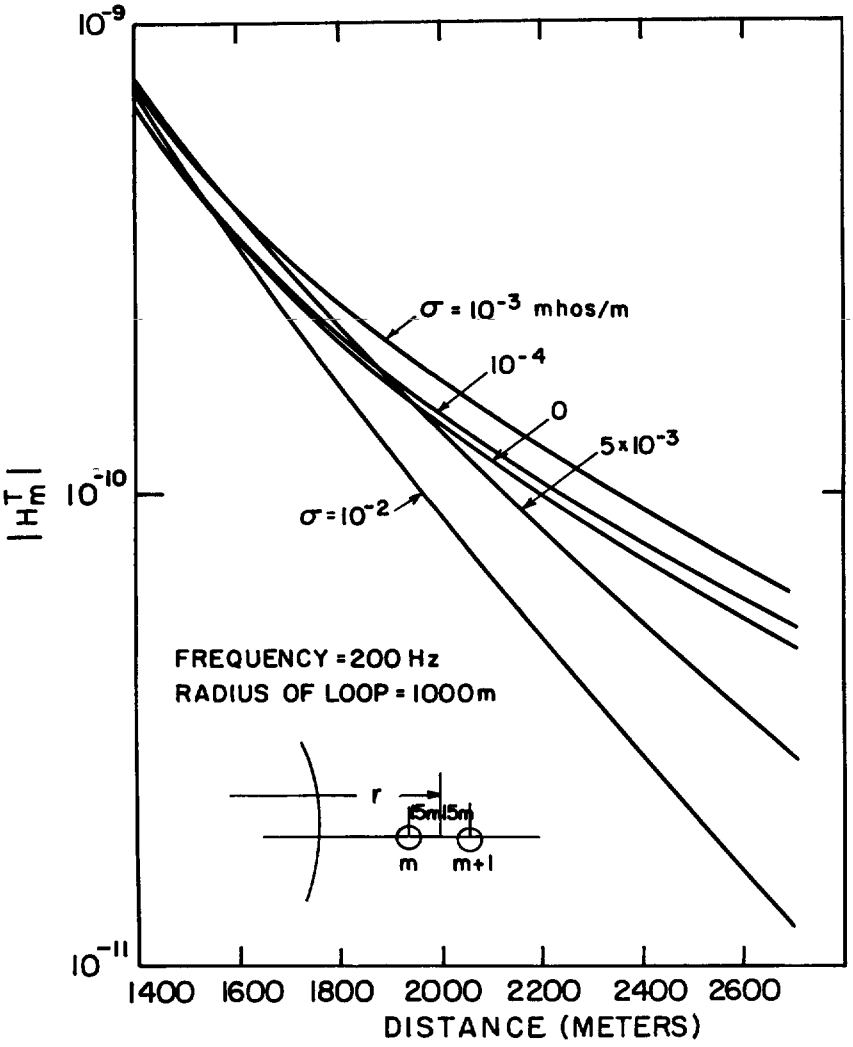

FIG. 30. Effect of ground conductivity on total vertical magnetic field for Turani.

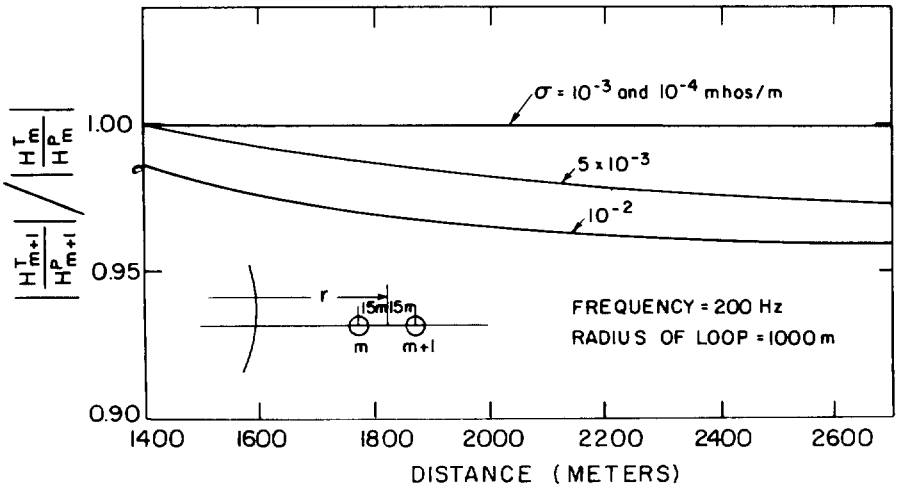

FIG. 31. Effect of ground conductivity on reduced ratio for Turam.

Frischknecht, F. C., 1967, Fields about an oscillating magnetic dipole over a two-layer earth and application to ground and airborne electromagnetic survey: Q. Colo. Sch. of Mines, v. 72, no. 1.

Gray, H. L., and Atchison, T. A., 1967, Nonlinear transformations related to the evaluation of improper integrals: I, SIAM. J. Numer. Analy., v. 4, p. 363–371.

Hohmann, G. W., and Ward, S. H., 1968, Electromagnetic depth sounding on lunar traverse: Proc. of AAS National Specialists Meeting on Water Resources of the Inner Planets, Las Vegas, Nevada, April 10–12.

Hood, P. J., and Sangster, D. F., 1967, The Carey Foster in-situ susceptibility meter: GSC, paper 65–22.

Kosenkov, O. M., 1963, The electromagnetic field of a circular loop at the earth-air boundary: Bull. Acad. Sci., USSR Geophysics Series, no. 12, p. 1120–1126.

Mooney, H. M., 1952, Magnetic susceptibility measurements in Minnesota: Part I, Technique of measurement: Geophysics, v. 17, p. 531–543.

Mooney, H. M., and Bleifuss, R., 1953, Magnetic susceptibility measurements in Minnesota, Part II, Analysis of field results: Geophysics, v. 18, p. 383–393.

Morrison, H. F., Phillips, R. J., and O'Brien, D. P., 1969, Quantitative interpretation of transient electromagnetic fields over a layered half-space: Geophys. Prosp., v. 21, p. 1–20.

Patra, H. P., 1967, Some studies on geoelectric sounding in engineering and hydro-geologic problems: Ph.D. dissertation, IIT, India.

Vanyan, L. L., 1967, Electromagnetic depth sounding: selected and translated by Keller, G. V., New York, Consultant Bureau.

Wait, J. R., 1951, The magnetic dipole over the horizontally stratified earth: Can. J. Phys., v. 29, p. 577–592.

——— 1952, Current-carrying wire loops in a single inhomogeneous region: J. Appl. Phys., v. 23, p. 497.

——— 1954, Mutual coupling of loops lying on the ground: Geophysics, v. 19, p. 290–296.

——— 1958, Induction by an oscillating, magnetic dipole over a two-layer ground: Appl. Sci. Res., v. 7, p. 73–80.

——— 1962, Theory of magnetotelluric fields: J. Res. NBS, Rad. Prop., v. 66D, p. 509–541.

Ward, S. H., 1967, Electromagnetic theory for geophysical application, *in* Mining Geophysics, v. 2: Tulsa, SEG.

——— 1969, Gross estimates of the conductivity, dielectric constant, and magnetic permeability distribution in the moon: Radio Science, v. 4, p. 117–139.

Watson, G. N., 1966, A treatise on the theory of Bessel functions, Second Ed., Cambridge, University Press.

Yoshizumi, E., Taniguchi, K., and Kiyono, T., 1959, Vertical sounding by central induction method: Memoirs of the Faculty of Engineering, Japan, Kyoto University.